2015

Bacterial sliding clamp inhibitors that mimic the sequential binding mechanism of endogenous linear motifs

Zhou Yin
University of Wollongong, zy877@uowmail.edu.au

Louise R. Whittell
University of Wollongong, lwhittel@uow.edu.au

Yao Wang
University of Wollongong, yw974@uowmail.edu.au

Slobodan Jergic
University of Wollongong, jergic@uow.edu.au

Cong Ma
University of Newcastle

See next page for additional authors

Publication Details

Yin, Z., Whittell, L. R., Wang, Y., Jergic, S., Ma, C., Lewis, P. J., Dixon, N. E., Beck, J. L., Kelso, M. J. & Oakley, A. J. (2015). Bacterial sliding clamp inhibitors that mimic the sequential binding mechanism of endogenous linear motifs. Journal of Medicinal Chemistry, 58 (11), 4693-4702.

Bacterial sliding clamp inhibitors that mimic the sequential binding mechanism of endogenous linear motifs

Abstract

The bacterial DNA replication machinery presents new targets for the development of antibiotics acting via novel mechanisms. One such target is the protein-protein interaction between the DNA sliding clamp and the conserved peptide linear motifs in DNA polymerases. We previously established that binding of linear motifs to the Escherichia coli sliding clamp occurs via a sequential mechanism that involves two subsites (I and II). Here, we report the development of small-molecule inhibitors that mimic this mechanism. The compounds contain tetrahydrocarbazole moieties as "anchors" to occupy subsite I. Functional groups appended at the tetrahydrocarbazole nitrogen bind to a channel gated by the side chain of M362 and lie at the edge of subsite II. One derivative induced the formation of a new binding pocket, termed subsite III, by rearrangement of a loop adjacent to subsite I. Discovery of the extended binding area will guide further inhibitor development.

Disciplines

Medicine and Health Sciences | Social and Behavioral Sciences

Publication Details

Yin, Z., Whittell, L. R., Wang, Y., Jergic, S., Ma, C., Lewis, P. J., Dixon, N. E., Beck, J. L., Kelso, M. J. & Oakley, A. J. (2015). Bacterial sliding clamp inhibitors that mimic the sequential binding mechanism of endogenous linear motifs. Journal of Medicinal Chemistry, 58 (11), 4693-4702.

Authors

Zhou Yin, Louise R. Whittell, Yao Wang, Slobodan Jergic, Cong Ma, Peter Lewis, Nicholas E. Dixon, Jennifer L. Beck, Michael J. Kelso, and Aaron J. Oakley

Bacterial Sliding Clamp Inhibitors that Mimic the Sequential Binding Mechanism of Endogenous Linear Motifs

Zhou Yin,[†,#] Louise R. Whittell,[†,#] Yao Wang,[†] Slobodan Jergic,[†] Cong Ma,[‡] Peter J. Lewis.[‡] Nicholas E. Dixon,[†] Jennifer L. Beck,[†] Michael J. Kelso,[†] and Aaron J. Oakley*[,†]

[†]School of Chemistry and Centre for Medical and Molecular Bioscience, The University of Wollongong, and The Illawarra Health and Medical Research Institute, Wollongong, New South Wales 2522, Australia

[‡]School of Environmental and Life Sciences, The University of Newcastle, Callaghan, New South Wales 2308, Australia

ABSTRACT: The bacterial DNA replication machinery presents new targets for the development of antibiotics acting *via* novel mechanisms. One such target is the protein–protein interaction between the DNA sliding clamp and the conserved peptide linear motifs in DNA polymerases. We previously established that binding of linear motifs to the *Escherichia coli* sliding clamp occurs *via* a sequential mechanism that involves two subsites (I and II). Here, we report the development of small-molecule inhibitors that mimic this mechanism. The compounds contain tetrahydrocarbazole moieties as "anchors" to occupy subsite I. Functional groups appended at the tetrahydrocarbazole nitrogen bind to a channel gated by the sidechain of M362 and lie at the edge of subsite II. One derivative induced the formation of a new binding pocket, termed subsite III, by rearrangement of a

loop adjacent to subsite I. Discovery of the extended binding area will guide further inhibitor development.

INTRODUCTION

New classes of antibiotics acting via novel mechanisms are urgently needed to combat increasing antibiotic resistance.[1-4] A rich source of potential new antibiotic targets is the bacterial DNA replisome.[5] During bacterial DNA replication and repair, the β-sliding clamp subunit (SC) of the DNA polymerase III (Pol III) holoenzyme, a ring-shaped homodimeric protein, encircles DNA and confers high processivity to DNA synthesis (Figure 1A).[6] Components of Pol III that interact with the SC at the same binding site include the α polymerase and ε proofreading subunits,[7] as well as the clamp loader (γ complex).[6] The variety of SC-focused interactions, the moderate number of SCs per cell (300–600 dimers),[8] the SC's conserved structure across bacterial species[9-11] and its structural divergence from the equivalent human protein (proliferating cell nuclear antigen, PCNA) [12, 13] make it an attractive target for antibiotic development.[5, 14]

Proteins that bind to the SC use short linear motifs (LMs, consensus sequence QLx_1Lx_2F/L: S/D preferred at x_1, x_2 may be absent)[15, 16] to interact with a LM-binding pocket consisting of two subsites (I and II),[17, 18] both of which are conserved across Gram-negative and Gram-positive species.[10] The two N-terminal residues of LMs bind in subsite II, while the two or three C-terminal residues occupy subsite I, with the linking residues filling a shallow channel between the sites. The side chain of SC residue M362

acts as a gate, transitioning from a "closed" (Figure 1B) to an "open" conformation (Figure 1C–E) upon binding of LM peptides.

We used structural, biochemical and computational techniques to identify that the interaction between LMs and the *E. coli* SC act *via* an 'anchor-based' sequential binding mechanism (Figure 1B–E).[19] Des-amino-Leu-Phe (dLF) was identified as a minimal SC-binding motif that occupies subsite I while maintaining M362 in the "closed" conformation (Figure 1B). In contrast, binding of AcLF stabilizes the "open" conformation of M362, accompanied by formation of a hydrogen bond between the acetylated N-terminal amide NH of the dipeptide and the carbonyl oxygen of G174 (Figure 1C). Binding of AcALDLF to the SC showed electron density for the three C-terminal residues only, which occupied subsite I and the channel while holding M362 in the "open" conformation (Figure 1D). Other pentapeptides, including AcQADLF (Figure 1E), were found to occupy subsite I, the channel and subsite II. We proposed that this series of peptide-bound SC structures captured the order of endogenous LM binding events: i.e., binding of dLF in subsite I mimics the primary binding contact, AcLF demonstrates subsequent formation of the H-bond to G174 with the M362 gate stabilized in the "open" conformation, and AcQADLF demonstrates binding of the N-terminal residues to subsite II by forming a network of hydrogen bonds to the glutamine side-chain amide.

According to the model, subsite I is the first point of contact between LM peptides and the SC, acting as the 'anchor site' for inhibitor binding. Two classes of non-peptidic small-molecule inhibitors, a thioxothiazolinine derivative[20] and a biphenyloxime ether[21]

have previously been shown to occupy subsite I (Supporting Information, Figure S1). Our recent fragment-based discovery efforts identified several new hits that also bind in subsite I.[22] Herein we report the design, synthesis, biochemical, biophysical and structural characterization of tetrahydrocarbazole (THC)-based inhibitors that mimic the 'anchor-based' sequential binding of LMs to the *E. coli* SC.

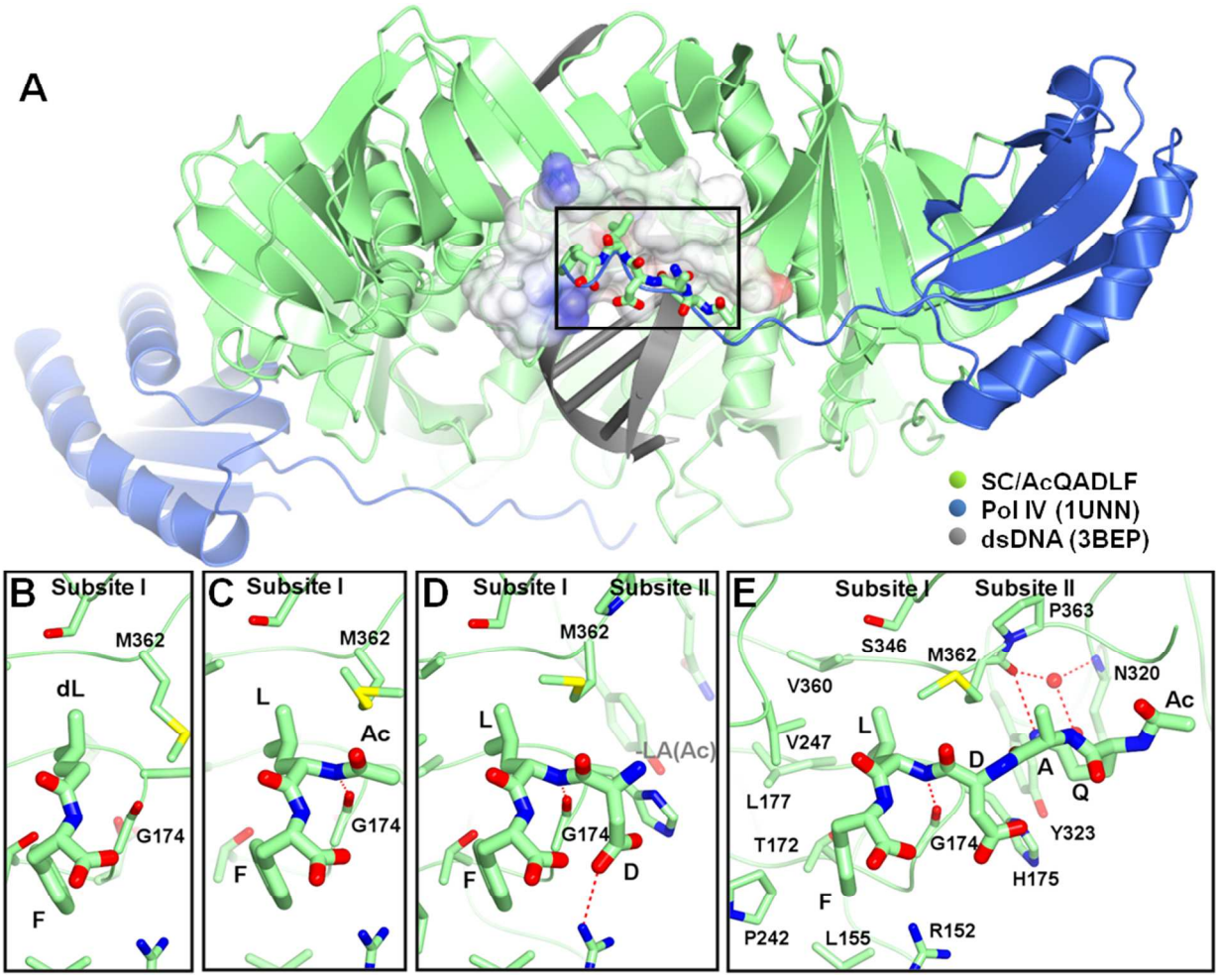

Figure 1. The sequential binding mechanism of LMs to the SC. (A) The *E. coli* SC structures in complex with pentapeptide AcQADLF (PDB entry 4K3O),[19] the SC binding-domain of Pol IV (1UNN)[18] and dsDNA (3BEP).[17] (B–E) X-ray co-crystal structures showing the binding of dLF, AcLF, AcALDLF (the AcAL–portion is disordered) and

AcQADLF to the SC binding pocket (PDB entries 4K3K, 4K3L, 4K3M and 4K3O, respectively).[19] Dashed lines in red represent H-bonds/salt bridges. A bridging water molecule is shown as a red sphere. Electrostatic potential surfaces in (A) are shown semi-transparent with blue = positive and red = negative.

RESULTS

A Tetrahydrocarbazole Lead Binds to Subsite I as a Mimic of the Anchor Motif. In previous work, we showed that the *R*-enantiomer of racemic tetrahydrocarbazole (THC) **1** (Figure 2) binds to subsite I of the *E. coli* SC.[22] Here, we explored optimization of THC binding to subsite I through substitution of the chlorine atom of **1** by other halogens and by shifting the carboxyl group to the 2-position of the cyclohexenyl ring (compounds **1a–j**, Figure 2). Our previously reported fluorescence polarization (FP)-based competition assay employing tracer peptide 5-carboxyfluorescein-QLDLF[20, 23, 24] was used to quantify binding of **1a–j** to the *E. coli* SC.[19] Inhibition of tracer binding was plotted against inhibitor concentration to generate IC_{50} values (Table 1 and Supporting Information, Figure S2), which were subsequently transformed into inhibition constants (K_i) using the Kenakin correction for ligand depletion (Table 1).[25] Ligand lipophilicity efficiency (LLE_{AT})[26] values were also calculated to inform inhibitor design, with LLE_{AT} values around 0.4 targeted (Table 1).

Racemic **1a** was obtained using standard Fisher indole chemistry from commercially available 4-chlorophenyl-hydrazine and (±)-3-oxocyclohexanecarboxylic acid (Figure 2). **1a** showed a K_i of 166 μM (Table 1). Esterification of **1a** (MeOH, H_2SO_4 (cat.)) provided

1b, while coupling of **1a** with ammonium hydroxide in the presence of 1-ethyl-3-(3-dimethylaminopropyl)carbodiimide (EDC) and *N*-hydroxy-succinimide (NHS) afforded amide **1c**. $LiAlH_4$ reduction of **1a** gave alcohol **1d**.[27, 28] However, none of **1b**–**d** was active (Table 1). The stereochemically pure *R* and *S* enantiomers of **1a** (i.e., **1e** and **1f**, respectively) were prepared using enantiomerically pure cyclohexane-3-carboxylic acids. Fluorinated (**1g**), iodinated (**1h**) and brominated analogues (**1i** and **1j**) were obtained with the appropriate 4-halophenylhydrazines and chiral cyclohexane-3-carboxylic acids. SC inhibition by **1e–j** indicated a preference for the *R*-enantiomer and chloro/bromo/iodo derivatives (Table 1).

Binding of racemic **1a** to the *E. coli* SC was examined using X-ray crystallography (see crystallographic data in Supporting Information, Table S1). Soaking **1a** into an *apo*-SC crystal resulted in only the *R*-enantiomer **1e** being observed in the electron density of the SC^{1e} complex (Figure 3), consistent with its higher SC affinity relative to **1f** (Table 1). **1e** was found to bind in subsite I of one chain (A) of the SC; the asymmetric unit contained a homodimer, chains A and B. Binding of **1e** to subsite I of chain B was also observed but a nearby crystal contact led us to consider the observed binding of **1e** to chain B to be less relevant (Supporting Information, Figure S3).

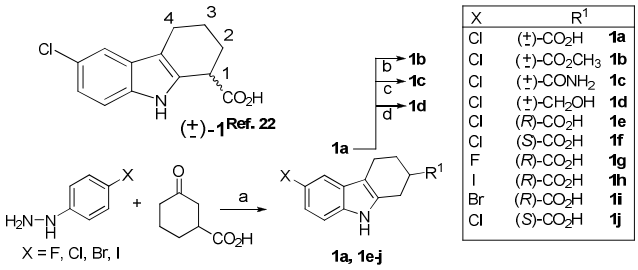

Figure 2. THCs (±)-**1** and **1a-j**. *Reagents and conditions*: (a) AcOH, reflux, (b) MeOH, H_2SO_4 (cat.), reflux, (c) (i) EDC/NHS, CH_2Cl_2, rt,(ii) NH_4OH, THF, (d) $LiAlH_4$, THF.

Table 1. Inhibition of the *E. coli* SC by 1a–j

	IC_{50} (μM)	K_i (μM)	cLogD (pH 7.2)	LLE_{AT}
1a	299	166	0.51	0.38
1b	>1000	–	–	–
1c	>1000	–	–	–
1d	>1000	–	–	–
1e	134	74	0.51	0.40
1f	442	246	0.51	0.36
1g	817	454	–0.11	0.39
1h	175	97	1.45	0.32
1i	157	87	0.83	0.37
1j	328	182	0.83	0.35

Binding of **1e** positioned the Cl-substituent deep within a hydrophobic pocket of the SC comprised of V247, V360, L177 and M362; the same region is occupied by the isobutyryl group of dLF (Figure 1B). The cyclohexenyl ring was observed to bind in the same shallow region (containing P242, T172 and L155) occupied by the Phe side chain of dLF. A significant difference between the two complexes was that the M362 gate remained "closed" (χ_2 = –173°, as observed in chain A of the equivalent *apo*-structure: PDB entry 1MMI[29]) upon binding of dLF (Figure 1B), whereas binding of **1e** stabilizes the "open" conformation of the M362 gate (χ_2 = –69°, Figure 3). The "open" conformation of M362 side-chain was previously identified during molecular dynamics simulation of the *apo*-SC crystal structure, but was only maintained as such when peptide ligands were bound.[19, 24]

Such The carboxylate group of **1e** made an H-bond interaction with the phenolic-OH of Y154 and a salt-bridge to the R152 guanidinium group. These additional interactions presumably contributed to the increased SC affinity of **1e** (K_i = 74 μM) relative to dLF (K_i > 1 mM).[19] Importantly, the NH group of **1e** projected towards the open M362 gate and associated channel, suggesting a synthetically tractable opportunity (i.e., via *N*-substitution) for directing additional functionality in the direction of subsite II and creating higher potency inhibitors that mimic the endogenous LM binding mechanism.

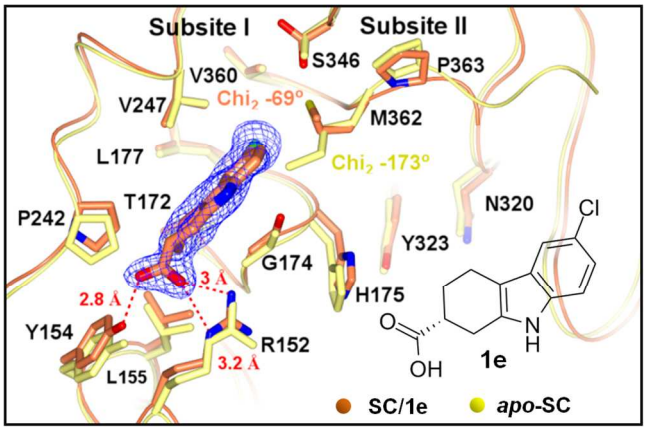

Figure 3. X-ray co-crystal structure of **1e** bound to subsite I of the *E. coli* SC (complex designated SC[1e]). Carbon atoms of the SC and **1e** are shown in orange and non-carbon atoms are colored according to CPK convention. The *apo*-SC structure (PDB entry 1MMI, chain A, shown in yellow) is superimposed onto SC[1e] for comparison. Pairs of atoms are indicated with dashed red lines. The electron density maps (2mF_o–DF_c) contoured at 1σ are shown in blue wire-basket form.

Inhibitors that Mimic the 'Anchor-Based' Sequential Mechanism of LM Binding to the *E. coli* SC. Visual inspection of the SC[1e] structure (Figure 3) suggested that addition of an acetamide group to the THC nitrogen of **1e** would position the appended amide NH in a region where it could potentially make an H-bond to the carbonyl oxygen of G174 – directly analogous to the H-bond observed in LM-SC complexes (Figure 1C–E). Enantiomeric *N*-acetamido-THCs **2a** and **2b** (carrying Cl-substituents) and the corresponding bromo-enantiomers **4a** and **4b** were synthesized as a test of this hypothesis. **2a** and **2b** were obtained in low yields (4–6%) *via* a 3-step procedure that involved conversion of acids **1e** and **1f** to ethyl esters (**1k** and **1l** respectively, Figure 4), *N*-alkylation of

the protected THCs with Cs_2CO_3/ ICH_2CONH_2 and final ester hydrolysis. The low alkylation yields with iodoacetamide led us to pursue an alternative sequence towards the bromo analogs **4a** and **4b**. Carboxylic acids **1i** and **1j** were first converted to their respective ethyl esters **1m** and **1n** and then *N*-alkylated with *tert*-butyl bromoacetate in the presence of Cs_2CO_3 in DMF. Removal of the *tert*-butyl group using neat TFA followed by EDC/NHS-mediated amidation with aqueous ammonia and final ethyl ester deprotection yielded **4a** and **4b** in 12% and 17% yields, respectively, over 4 steps.

Compounds **2a** and **4a** showed higher affinity for the SC than their enantiomeric counterparts **2b** and **4b**, again reflecting the preference for *R*-stereochemistry at the ring carboxylic acid (Table 2). The co-crystal structure of the SC with **2a** (Figure 5A, complex denoted SC^{2a}; see crystallographic data in Supporting Information, Table S2) showed that the binding pose of **2a** is similar to **1e** (Figure 3). The conformational changes in the side chains of S346 and M362 upon binding of **1e** were also observed with **2a** and, crucially, it was found that the amide-NH of **2a** formed the expected H-bond to the carbonyl oxygen of G174. Additionally, as observed with the similarly sized dipeptide AcLF (Figure 1C), formation of this H-bond coincided with opening of the M362 gate, in agreement with our anchor-based sequential binding model.[19] The binding mode of **2a** suggested that further potency increases might be achieved with *N*-substituted acetamides, which could similarly trigger opening of the M362 gate and formation of the H-bond to G174 while simultaneously projecting additional functionality across the channel towards subsite II to mimic the SC-binding mechanism of LMs.

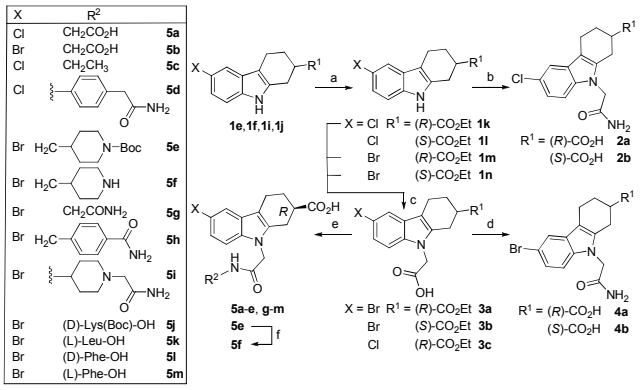

Figure 4. Synthesis of *N*-acetamido-THCs. *Reagents and conditions*: (a) EtOH, H_2SO_4 (cat.), reflux; (b) (i) ICH_2CONH_2, Cs_2CO_3, DMF, 80°C, (ii) NaOH, EtOH, rt; (c) (i) *tert*-butyl bromoacetate, Cs_2CO_3, DMF, 80°C, (ii) TFA; (d) (i) EDC/NHS, CH_2Cl_2, rt, (ii) $NH_4OH_{(aq)}$, THF, (iii) LiOH, THF, rt; (e) (i) NH_2-R_2, HATU, DIPEA, DMF, rt, (ii) NaOH or LiOH, EtOH, rt; (f) neat TFA.

Table 2. Inhibition of the *E. coli* SC by *N*-Acetamido-THCs

	IC_{50} (μM)	K_i (μM)	LogD (*p*H 7.2)	LLE_{AT}
2a	368	204	–0.75	0.40
2b	888	493	–0.75	0.38
4a	246	137	–0.73	0.41
4b	285	158	–0.73	0.41
5a	85	47	–4.76	0.61

5b	20	11	–4.63	0.64
5c	347	193	0.01	0.33
5d	362	201	0.20	0.27
5e	150	83	1.23	0.22
5f	208	116	–1.00	0.35
5g	171	95	–1.79	0.43
5h	64	36	0.18	0.30
5i	307	171	0.27	0.27
5j	115	64	–3.26	0.40
5k	48	27	–3.57	0.50
5l	30	17	–3.19	0.45
5m	27	15	–3.19	0.45

Aspartate or glutamate residues are often present in SC-binding LMs, serving as bridging residues that occupy the channel region between subsites I and II (Figure 1D–E). [15, 19, 24] We predicted that glycinamides **5a** and **5b** (Figure 4) would position their Gly carboxylate groups into the region occupied by LM Asp and Glu side chains. To test this, **5a** and **5b** were prepared in modest yields (10–40%) from their precursor ethyl esters **3a** and **3c** by first coupling glycine methyl ester using standard amide coupling conditions (HATU, DIPEA, DMF) and then simultaneously hydrolyzing the methyl and ethyl esters with base. The precursor ester **3c** was prepared as for **3a** from 4-chlorophenylhydrazine in

59% yield over 4 steps (Figure 4). **5a** and **5b** both contained *R*-configured carboxylates at the 2-position. The *S*-enantiomers of **5a** and **5b** (and other inhibitors) were not investigated beyond this point due to the lower SC affinity observed (Tables 1 and 2). The bromo-acid analog **5b** showed higher potency (K_i = 11 μM, Table 2) relative to the corresponding primary amide **4a** (K_i = 137 μM) and the chloro-analog **5a** (K_i = 47 μM). These results led us to focus subsequent efforts on bromo-THCs.

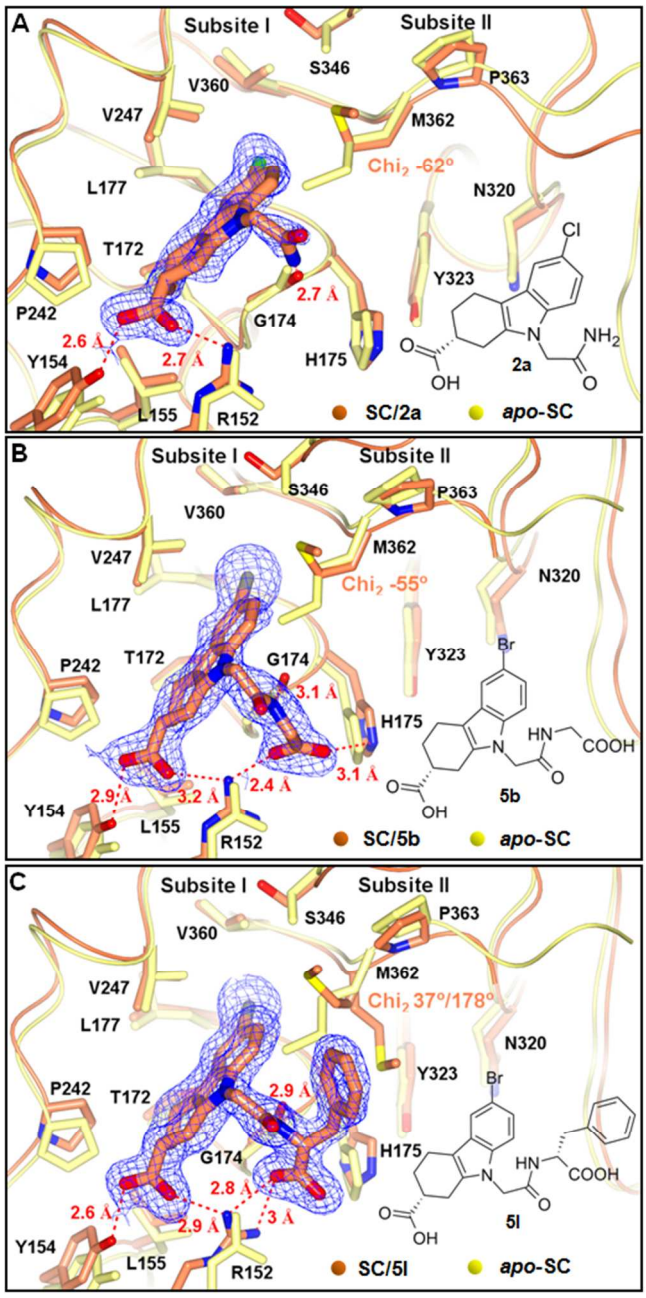

Figure 5. X-ray co-crystal structure of (A) **2a**, (B) **5b** and (C) **5l** bound to the *E. coli* SC (complexes designated SC^{2a}, SC^{5b} and SC^{5l}, respectively). The complexes are represented with carbon atoms shown in orange and non-carbon atoms following CPK convention. The *apo*-SC structure (PDB entry 1MMI, chain A, shown in lemon) is superimposed on each complex for comparison. Inhibitor electron density maps ($2mF_o–DF_c$) contoured at 1σ are shown in blue wire-basket form.

A co-crystal structure of the SC with **5b** (Figure 5B, complex denoted SC^{5b}; see crystallographic data in Supporting Information, Table S1) showed that **5b** made all of the same SC interactions as **2a** (Figure 5A). The appended glycine carboxylate of **5b**, however, made additional hydrogen bond/salt bridge contacts with the side chains of R152 and H175, thus explaining its higher potency relative to its parent amide **4a**. As expected, the glycyl group occupied the channel region between subsites I and II, mimicking the channel-binding Asp residues in LMs (Figure 1D, E). **5c–i** (Figure 4), synthesized in variable yields (4–64%) using similar methods, were found to have reduced potency relative to **5b** (Table 2). Amino acid-containing compounds **5j–m** were examined next to explore whether side chains appended to the **5b** glycine α-carbon could occupy subsite II. **5l** and **5m** were prepared in moderate yields (30–57%) via amide coupling reactions of D- and L-phenylalanine methyl esters with **3a**, respectively, followed by global methyl/ethyl ester deprotection using base (Figure 4). Both **5l** and **5m** (K_i = 17 and 15 μM, respectively, Table 2) showed similar SC affinities to **5b** (K_i = 11 μM, Table 2).

A co-crystal structure of the SC with **5l** (Figure 5C, complex denoted SC^{5l}; crystallographic data in Supporting Information, Table S1) showed that the overall binding pose of **5l** was similar to that of **5b** (Figure 5B). **5l** extended to the edge of subsite II where its phenyl ring occupied part of the space filled by LM peptide sub-motifs (Figure 1E). The M362 side chain adopted alternate conformations upon binding of **5l**, one where it displayed the usual "open" state whilst in the other it was shifted towards subsite II due to an interaction with the phenyl ring.

The binding of inhibitors **1e**, **2a**, **5b** and **5l** to the *E. coli* SC closely matched our 'anchor'-based LM sequential binding mechanism.[19] Compound **1e** is positioned as an 'anchor' in subsite I. Having the same THC moiety anchored in subsite I, compounds **2a**, **5b** and **5l** maintained the M362 gate in the open conformation and made the H-bond interaction with G174– features uniformly observed in LM-bound SC structures. It therefore seems likely that binding of **2a**, **5b** and **5l** (and probably other THC-based inhibitors) would invoke the sequential binding mechanisms of LMs; i.e., where the THC group makes initial contact with subsite I, captures the "open" state of the M362 gate and then redirection of the appended groups occurs leading to formation of the G174 H-bond. This assertion is supported by the poses adopted by **2a** and **5l** when bound to the SC chain B (Supporting Information, Figure S3). Inhibitor binding to chain B beyond subsite I is impeded by the presence of the SC symmetry partner – a crystallographic artefact. In these structures, **2a** and **5l** positioned their THC moieties in subsite I but their appended groups were shunted away from the channel and subsite II into solvent by the crystallographic symmetry partner.

Ligand-Induced Loop Rearrangement Creates an Additional Binding Pocket. The observation of similar SC binding affinities for diastereomers **5l** and **5m** (containing D- or L-Phe moieties, respectively) led us to investigate the binding pose adopted by **5m**. SC/**5m** co-crystal structures were solved (denoted $SC^{\mathbf{5m}}$, Figure 6A; crystallographic data in Supporting Information, Table S2) and the *apo*-SC structure with similar cell dimensions was also solved for comparison (denoted SC^{apo}; crystallographic data in Supporting

Information, Table S2). **5m** was observed to bind to chain B of this SC crystal with its THC unit occupying subsite I, as observed with other THCs. The symmetry partners that had occupied the channel region and subsite II of chain B in other SC crystals of smaller cell dimensions were not observed with this structure. The binding of **5m** caused similar conformation changes in the side chains of S346 and M362 to those observed in other THC-SC structures; however, a dramatic rearrangement in the loop region comprising H148–Y154 was induced upon binding of **5m** (Figure 6A; additional electron density maps highlighting the differences between the loop regions of SC^{apo} and $SC^{\mathbf{5m}}$ are provided in Supporting Information, Figure S4). While the H148 and Y154 residues at the start and end of the loop had undergone minor changes in their side chain conformations, the residue pair of Q149 and D150 had exchanged positions. The residue pair of R152 and Y153 had also exchanged positions and V151, located in the middle of the loop, had moved to accommodate these changes.

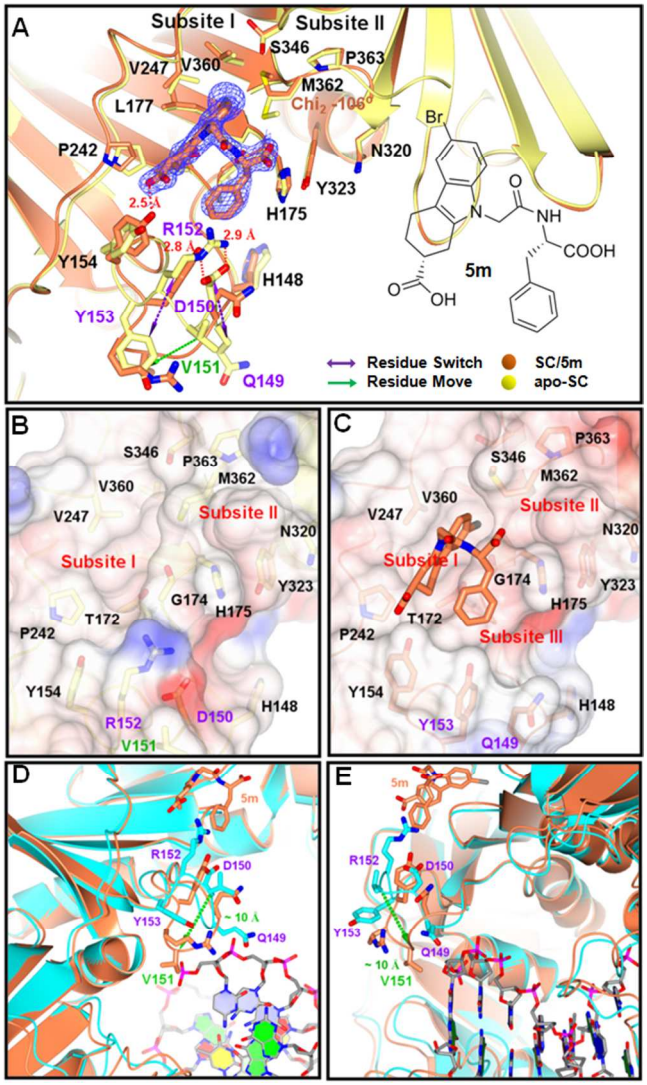

Figure 6. Co-crystal structure of **5m** bound to the *E. coli* SC. (A) SC^{5m} is displayed with carbon atoms in orange and non-carbon atoms colored according to CPK convention. The SC^{apo} structure is superimposed onto SC^{5m} for comparison (carbon atoms colored yellow and non-carbon atoms in CPK colors). Hydrogen bonds are indicated with dashed red lines. Purple and green arrows indicate movement of SC residues in the SC^{apo} *vs.* SC^{5m} structure. Electron density maps ($2mF_o$–DF_c) contoured at 1σ are shown in blue wire-basket form. (B and C) Electrostatic potential surfaces of the binding sites in SC^{apo} and SC^{5m} shown in semi-transparent form (blue = positive; red = negative). (D and (E) Struc-

tural overlap of SC^{5m} and dsDNA-bound SC (PDB entry 3BEP) with carbon atoms in orange and cyan respectively. Atoms of DNA molecules are in CPK colors and the nucleic acid bases are also represented as blocks (A: red, G: green, T: yellow, C: blue). The dsDNA axis is directed at the viewer in (D) and the system is rotated 90° clockwise in (E).

The loop rearrangement significantly altered the surface geometry and electrostatics in this region of the SC (Figures 6B and C). The charged area originally occupied by the side chains of R152 and D150 and the surrounding residues G174, Y154 and H175 in SC^{apo} were replaced by neutral residues Y153 and Q149 in SC^{5m} to accommodate the hydrophobic phenyl ring of **5m**. We denote the new ligand-induced binding area, comprising G174, Y154, Y153, Q149 and H175 as "subsite III". It is of note that the phenyl group of **5m** occupied only half of subsite III, leaving the area between H175 and Q149 vacant and potentially available for further targeting.

Sequence alignments comparing the LM binding pockets and H148–Y154 loop regions of SCs from representative Gram-negative (*E. coli*, *Acinetobacter baylyi*, *A. baumannii* and *Pseudomonas aeruginosa*) and Gram-positive (*Staphylococcus aureus*, *Bacillus subtilis*, *Streptococcus pneumoniae* and *S. pyogenes*) species (Supporting Information, Figure S5) show that the switching residue pairs in the loop region (i.e., Q149–D150 and R152–Y153), along with V151, are well conserved across the Gram-negatives, but less so among the Gram-positives. This suggests that the ligand-induced loop rearrangement may be a feature common to Gram-negative species. The conformational change is also of interest because the rearranged loop is located at the inner edge of the SC dimer in the

region through which dsDNA passes (Figure 4D, E). The ~10 Å movement of V151 towards the center of the ring positioned it where dsDNA would be expected to bind (see PDB entry 3BEP).[17] The movements in several residues involved in both the binding of **5m** and ssDNA/dsDNA shows that this region is open to remodeling by ligands.In addition to inhibiting LM binding, **5m** may also act as an inhibitor of the SC/DNA interaction. This hypothesis may in part be corroborated by the *E. coli* SC-DNA complex crystal structure, [17] which demonstrated side-chain movement of Q149 upon dsDNA binding due to steric hindrance, and residues Y153 and Y154 interacting with a nearby ssDNA segment from a symmetry-related molecule.

Dissociation Constants of Complexes of THC Derivatives with the *E. coli* SC. Thermodynamic data for the binding of THCs **5a**, **5b**, **5l** and **5m** to the *E. coli* SC were obtained using isothermal titration calorimetry (ITC). In all cases the observed dissociation constants, K_d (Table 3 and Supporting Information Figure S6) matched well the K_i values obtained from the fluorescence polarization assays (Table 2; Supplementary Information, Figure S2). The thermodynamic profiles (ΔH and $-T\Delta S$ values) for each inhibitor were also similar, consistent with their closely related binding poses in subsite I. Interestingly, the loop rearrangement induced in the SC upon binding of **5m** did not significantly alter the enthalpy or entropy of binding relative to other inhibitors.

Table 3. ITC Data (298 K) for the Binding of THC Derivatives to the *E. coli* SC

	ΔH (kcal/mol)	$-T\Delta S$ (kcal/mol)	ΔG (kcal/mol)	K_d (μM)
5a	–13.2 ± 0.16	6.8	–6.3	24 ± 2
5b	–15.1 ± 0.12	8.5	–6.6	14 ± 0.9
5l	–12.0 ± 0.1	5.3	–6.6	13 ± 1
5m	–13.7 ± 0.13	6.8	–6.9	9 ± 0.8

THC Derivatives Inhibit *in vitro* DNA Replication. DNA replication assays were used to demonstrate inhibition of *E. coli* SC function by THC derivatives **1e**, **1i**, **2a**, **4a**, **5a**, **5b**, **5l** and **5m**. Briefly, circular ssDNA with an RNA primer was used as template in a minimized reaction system containing the SC, single-stranded DNA-binding protein (SSB), the Pol III α subunit and the reconstituted $\gamma_3\delta\delta'$ clamp loader complex.[30] In this system purposely minimized to avoid potentially confounding effects of inhibitors on other protein–protein interactions in more efficient full-replisome systems,{Jergic, 2013 #238} the SC is loaded onto the primed DNA by the clamp loader complex, which is subsequently released.[17, 31, 32] Binding of the α subunit leads to extension of the primer through incorporation of dNTPs using the primed ssDNA as template[33, 34] (see Supporting Information, Figures S7 and S8 for a schematic representation of the assay and a control experiment). Binding of the DNA Pol III δ and α subunits to the SC is essential for DNA replication to occur in this system and is impaired by the presence of inhibitors. In-

hibition of SC binding leaves residual ssDNA templates and incomplete dsDNA products, whereas successful synthesis yields complete dsDNA products (Figure 7).

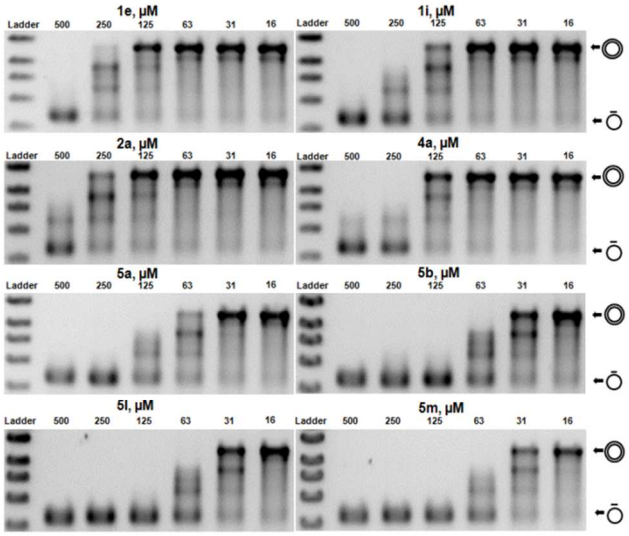

Figure 7. Inhibition of *E. coli* SC-mediated *in vitro* DNA replication by **1e**, **1i**, **2a**, **4a**, **5a**, **5b**, **5l** and **5m**. DNA laddersindicate 8, 6, 5, 4 and 3 kilobase pairs of DNA in each panel (top to bottom). Ladder = DNA molecular size standards. Circles with a short line above represent RNA-primed ssDNA templates. Two concentric circles represent completed dsDNA synthesis products.

Compounds **1e**, **1i**, **2a** and **4a** inhibited DNA replication at concentrations >125 μM (Figure 7), consistent with their relatively weak SC affinities (K_i = 74–204 μM, Tables 1 and 2). Compounds **5a** (K_i = 47 μM) inhibited DNA replication at concentrations >63 μM, while **5b** (K_i = 11 μM), **5l** (K_i = 17 μM) and **5m** (K_i = 15 μM) all showed inhibitory effects at 31 μM, consistent with their higher SC affinities.

DISCUSSION

A characteristic feature of linear motif (LM) recognition by the *E. coli* sliding clamp (SC) is separation of the LM binding pocket on the SC surface into two distinct subsites (subsites I and II), with an intervening channel region gated by the side chain of M362. Subsite I acts as the anchor site for binding of 'anchor motifs' in the consensus sequences of partner proteins.[19] All SC inhibitors identified to date bind in subsite I. Our sequential binding model[19] describes how binding events at the channel region and subsite II occur only after ligands are first 'anchored' into subsite I. Tetrahydrocarbazole (THC) derivatives **1e** and **1i** were identified as ligands that act as anchor moieties in subsite I, while at the same time positioning their THC nitrogen in an orientation that allowed additional functionality to be added and projected into the channel towards subsite II, thus matching the binding mechanism of LM consensus peptide ligands. The hydrogen bond with G174 and the "open" conformation of the M362 gating residue, which are both consistently observed upon LM peptide binding, were reproduced by members of the *N*-linked THCs, exemplified by **2a**, **5b** and **5l** (Figure 5). Compound **5l** was found to occupy subsite I, the channel region and the edge of subsite II, providing valuable insights for future work to, for example, extend inhibitors farther into subsite II by substituting the phenyl ring of the D-phenylalanine moiety or by replacing it with other functionalized D-amino acids.

The binding of **5m** to the *E. coli* SC induced a loop rearrangement that resulted in positional switching of residue pairs Q149–D150 and R152–Y153 and a 10 Å movement of V151. To our knowledge, no peptides or synthetic entities that bind the SC (including the clamp-loader complex, which can pry open the SC dimer ring)[17] have been observed to

exert such allosteric effect. This ligand-induced rearrangement revealed a hitherto unreported binding pocket, which we denote 'subsite III'. Compound **5m** did not form the hydrogen bond with G174 observed with other THC derivatives (Figure 6A), nor did its carboxylate group make interactions with R152 and H175 (as observed with **5b** and **5l**; Figure 5B and C). Nonetheless, **5m** displayed similar SC affinity to **5b** and **5l**, suggesting that the SC conformational changes and occupancy of subsite III by **5m** contributed favorably to binding (Figure 6C). Subsite III therefore appears as an attractive 'ligand-induced' site for targeting through further substitution of **5m** or related structures. Compounds of this type have potential to inhibit the SCs of Gram-negative bacteria in particular, due to their well conserved subsite I and loop residues H149–Y153. The possibility that **5m** and associated derivatives might also modulate SC–DNA interactions is intriguing but remains to be investigated.

THC derivatives **5b**, **5l** and **5m** showed >10-fold increases in SC affinity relative to initial hit **1a**, and also have increased LLE_{AT} values. The previously described thioxothiazolinine derivative and biphenyloxime derivative SC inhibitors (Supporting Information, Figure S1) bound to subsite I and showed affinities >10 μM. THC derivatives **5l** and **5m** displayed similar SC affinities achieved through expanded binding site coverage to compensate reduced ligand efficiency, with **5l** extending to the edge of subsite II and **5m** revealing the new subsite III. Both compounds provide synthetically accessible possibilities for evolving further generations of inhibitors that fully occupy subsites I and II or III and show increased potency.

Binding of these *N*-substituted THCs was in good agreement with the anchor-based sequential binding mechanism proposed for SC-binding LM peptides.[19] The substituted THC anchor motifs occupied subsite I first, followed by positioning of the rest of the ligand. This observation may be generally applicable for development of inhibitors of LM binding, since other LMs may also possess key 'anchor' residues that drive binding to partner proteins.[35, 36] Similar inhibitor design strategies may be successful when applied in evolutionarily related and/or biochemically similar systems. For example, the eukaryotic SC homolog, PCNA, that mediates interactions in eukaryotic DNA replication *via* recognition of a Qxx[I/L]xxFF motif,[12] has been suggested as an anticancer target.[37] Targeting 'anchor sites' and adjacent areas in this (and other) systems, after delineating the mechanisms of LM recognition, may serve as an effective strategy for inhibitor design.

MATERIALS AND METHODS

Chemo-informatics, Bioinformatics and Organic Synthesis. Compounds were ≥ 95% pure as confirmed by ^{1}H NMR. Full details are given in the Supporting Information.

Protein Expression and Purification. Expression and purification of the *E. coli* SC, Pol III α subunit, SSB and the $\gamma_3\delta\delta$' clamp loader complex were as described previously.[16, 30, 38]

Crystallization and X-Ray Data Collection. Crystals of the *E. coli* SC were grown at 285 K by the hanging-drop vapor diffusion method. The hanging drop was composed of 1 µl of sliding clamp (53 mg/mL in 10 mM Tris-HCl pH 7.2, 1 mM dithiothreitol, 1 mM EDTA and 15% glycerol) mixed with an equal volume of reservoir solution consisting of

100 mM MES pH 6.5, 100–150 mM $CaCl_2$ and 25–30% (v/v) PEG400. The reservoir volume was 1 mL. SC crystals were transferred to a $CaCl_2$-free reservoir and ligands were soaked into the crystal at 2–5 mM in reservoir solution with <10% DMSO. All crystals were mounted using MiTeGen loops on pins with magnetic caps. For in-house data collection, crystals were flash-frozen at 100 K using an Oxford Cryo-stream. Diffraction data were collected using a Mar345 desktop beamline using CuKα X-rays from a Rigaku 007HF rotating anode generator with Varimax optics. For synchrotron data collection, the SSRL automated mounting system (SAM) was used. Mounted crystals were flash-frozen in liquid nitrogen and placed in the SAM cassettes. Diffraction data were collected at 100 K at the Australian Synchrotron, Beamline MX1 using X-rays of wavelength 0.95 Å.

Data Processing, Structure Solution and Refinement. Crystal data sets were integrated, merged and scaled with HKL2000[39] or MOSFLM and SCALA.[40] The structures were solved by molecular replacement with CCP4 using the Protein Data Bank entry 1MMI[29] or 4K3S[19] as the starting model. Iterative cycles of model building and refinement were performed in COOT[41] and REFMAC5. [42]

Fluorescence Polarization Assay. Experiments and data processing protocols were reported previously.[19] All FP experiments were conducted using a POLARstar Omega plate reader with non-treated black sterile 96-well plates (Greiner, USA). The buffer contained 10 mM HEPES pH 7.4, 1 mM EDTA, 1 mM dithiothreitol, 0.07% Nonidet P-40 and 5% DMSO. The fluorescent tracer used was *N*-fluorescein (FAM)-QLDLF-OH (GL Biochem, China), which has a K_d of 70 nM for SC monomers. For the competition assay, 10

nM peptide and 50 nM sliding clamp (as monomers) were used. Blank control (buffer), negative control (buffer and the peptide) and positive control (buffer, peptide and the sliding clamp) were used for data normalization. Data are shown as % inhibition relative to maximum, calculated as the decrease in polarization from maximum divided by the background-subtracted total polarization. Experiments were carried out in duplicate. Curves were fit using GraphPad Prism v5.01 (GraphPad Software, USA) and data are presented as "best-fit" values. Dose-response curve fitting was applied to competition assays with variable slope.

Isothermal Titration Calorimetry. ITC used a MicroCal Auto-iTC200 calorimeter (GE Healthcare) at 298 K. The SC was dialyzed against a buffer (10 mM HEPES pH 7.2, 0.15 M NaCl and 1 mM EDTA) and the same buffer was used to dissolve the compounds. The feedback mode was “high” with a reference power setting of 10 μcal/s. The cell was stirred at 1000 rpm and the thermostat set at 25 °C. Experiments were conducted with 19 injections of 2 μL over 4s with 200s intervals between injections. The first injection (of 0.4 μL) was discarded in all cases. Compounds (0.7-1 mM) were titrated in sequential injections into 75 μM SC monomer. Data were corrected for control experiments with compounds titrated into buffer only. Data analysis was carried out with Origin 7.0 using one-site binding data fitting.

DNA replication assay. The RNA-primed DNA template was prepared in advance by mixing 35 nM wild-type M13 ssDNA[26] with 1 μM oligoribonucleotide (5’-UAUGUACC-CCGGUUGAUAAUCAGAAAAGCCCCA; GeneWorks, Australia) in 30

mM Tris-HCl pH 7.6, 15 mM $MgCl_2$, 130 mM NaCl and 0.1 mM EDTA for 10 min at 55 °C and cooling to room temperature over a period of 8 h. The DNA replication assays contained: 20 mM Tris-HCl pH 7.6, 10 mM $MgCl_2$, 0.8 mM ATP, 8.4 mM dithiothreitol, 0.6 mM of each dNTP, 50 nM Pol III α subunit, 700 nM SSB (as tetramers), 210 nM Pol III β sliding clamp (as dimers), 42 nM $\gamma_3\delta\delta'$ clamp loader complex, 120 mM NaCl and 3 nM RNA primed DNA template, in a volume of 15 μL. Inhibitors (peptides or THC derivatives) were dissolved in DMSO and diluted in series 2-fold (in 50% v/v DMSO) before being added (0.5 μL) to the assay mixture at 0°C. The final DMSO concentration was 3.4% (v/v) in all assays. The assay mixtures were treated at 30 °C for 60 min before being quenched by the addition of EDTA to 150 mM and SDS to 1% (w/v). The DNA products were separated by 0.7% agarose gel electrophoresis in TAE buffer (80 mM Tris, 40 mM acetic acid, and 4 mM EDTA) and then stained with 10,000-fold diluted SYBR Gold (Life Technologies) for 60 min. The DNA products were visualized using a UV transilluminator.

ASSOCIATED CONTENT

Supporting Information

Supplementary figures, crystallographic data, supplementary methods of chemoinformatics, bioinformatics and organic synthesis. This material is available free of charge via the Internet at http://pubs.acs.org.

Accession codes

The atomic coordinates and structure factors for SC^{1e}, SC^{2a}, SC^{5b}, SC^{5l}, SC^{apo} and SC^{5m} have been deposited in the Protein Data Bank with accession codes 4OVF, 4OVG, 4OVH, 4PNU, 4PNV and 4PNW, respectively.

AUTHOR INFORMATION

Corresponding Author

*Email: aarono@uow.edu.au; phone: +61-42214347

Author Contributions

[#]Z.Y. and L.R.W. contributed equally to this work.

Notes

The authors declare no competing financial interest.

ACKNOWLEDGMENTS

This research was supported by the Australian Research Council (ARC) Discovery Project DP110100660 and the National Health and Medical Research Council (Australia) Project Grant 1021479. A.J.O. acknowledges support from the ARC for his Future Fellowship (FT0990287). We acknowledge the work of Thomas O'Meley, who contributed to the preparation of compound **5k**. Some of the reported X-ray diffraction data were collected at the Australian Synchrotron, Beamline MX2.

ABBREVIATIONS USED

dNTP, deoxyribonucleoside triphosphate; dsDNA, double-stranded DNA; dLF, desamino-Leu-Phe; DMF, dimethylformamide; DIPEA, *N*,*N*-diisopropylethylamine; EDC, 1-ethyl-3-(3-dimethylaminopropyl)carbodiimide; FP, fluorescence polarization; HATU, *N*-[(dimethylamino)-1*H*-1,2,3-triazolo-[4,5-*b*]pyridin-1-ylmethylene]-*N*-methylmethanaminium hexafluorophosphate *N*-oxide**;** IC_{50}, half-maximum inhibitory concentration; K_i, inhibition constant; LogD, distribution coefficient; LE, ligand efficiency; LLE_{AT}, ligand lipophilicity efficiency; LM, linear motif; NHS, *N*-hydroxysuccinimide; PCNA, proliferating cell nuclear antigen; PDB, protein data bank; Pol, polymerase; SC, sliding clamp; ssDNA, single-stranded DNA; TFA, trifluoroacetic acid; THC, tetrahydrocarbazole.

REFERENCES

(1) Spellberg, B.; Bartlett, J. G.; Gilbert, D. N. The future of antibiotics and resistance. *N. Engl. J. Med.* **2013**, *368*, 299–302.

(2) Coates, A. R. M.; Halls, G.; Hu, Y. Novel classes of antibiotics or more of the same? *Br. J. Pharmacol.* **2011**, *163*, 184–194.

(3) Devasahayam, G.; Scheld, W. M.; Hoffmann, P. S. Newer antibacterial drugs for a new century. *Expert Opin. Investig. Drugs* **2010**, *19*, 215–234.

(4) Moellering, R. C., Jr. Discovering new antimicrobial agents. *Int. J. Antimicrob. Agents* **2011**, *37*, 2–9.

(5) Robinson, A.; Causer, R. J.; Dixon, N. E. Architecture and conservation of the bacterial DNA replication machinery, an underexploited drug target. *Curr Drug Targets* **2012**, *13*, 352–372.

(6) Stukenberg, P. T.; Studwell-Vaughan, P. S.; O'Donnell, M. Mechanism of the sliding β-clamp of DNA polymerase III holoenzyme. *J Biol Chem* **1991**, *266*, 11328–11334.

(7) Ozawa, K.; Horan, N. P.; Robinson, A.; Yagi, H.; Hill, F. R.; Jergic, S.; Xu, Z. Q.; Loscha, K. V.; Li, N.; Tehei, M.; Oakley, A. J.; Otting, G.; Huber, T.; Dixon, N. E. Proofreading exonuclease on a tether: the complex between the E. coli DNA polymerase III subunits α, ε, θ and β reveals a highly flexible arrangement of the proofreading domain. *Nucleic Acids Res* **2013**, *41*, 5354–53567.

(8) Leu, F. P.; Hingorani, M. M.; Turner, J.; O'Donnell, M. The δ subunit of DNA polymerase III holoenzyme serves as a sliding clamp unloader in Escherichia coli. *J Biol Chem* **2000**, *275*, 34609–34618.

(9) Burnouf, D. Y.; Olieric, V.; Wagner, J.; Fujii, S.; Reinbolt, J.; Fuchs, R. P. P.; Dumas, P. Structural and biochemical analysis of sliding clamp/ligand interactions suggest a competition between replicative and translesion DNA polymerases. *J. Mol. Biol.* **2004**, *335*, 1187–1197.

(10) Argiriadi, M. A.; Goedken, E. R.; Bruck, I.; O'Donnell, M.; Kuriyan, J. Crystal structure of a DNA polymerase sliding clamp from a Gram-positive bacterium. *BMC Struct. Biol.* **2006**, *6*, 2.

(11) Gui, W. J.; Lin, S. Q.; Chen, Y. Y.; Zhang, X. E.; Bi, L. J.; Jiang, T. Crystal structure of DNA polymerase III β sliding clamp from *Mycobacterium tuberculosis*. *Biochem. Biophys. Res. Commun.* **2011**, *405*, 272–277.

(12) López de Saro, F. J.; Georgescu, R. E.; Goodman, M. F.; O'Donnell, M. Competitive processivity-clamp usage by DNA polymerases during DNA replication and repair. *EMBO J.* **2003**, *22*, 6408–6418.

(13) Indiani, C.; O'Donnell, M. The replication clamp-loading machine at work in the three domains of life. *Nat. Rev. Mol. Cell. Biol.* **2006**, *7*, 751–761.

(14) López de Saro, F. J. Regulation of interactions with sliding clamps during DNA replication and repair. *Curr Genomics* **2009**, *10*, 206-215.

(15) Dalrymple, B. P.; Kongsuwan, K.; Wijffels, G.; Dixon, N. E.; Jennings, P. A. A universal protein-protein interaction motif in the eubacterial DNA replication and repair systems. *Proc. Natl. Acad. Sci. U.S.A.* **2001**, *98*, 11627–11632.

(16) Wijffels, G.; Dalrymple, B. P.; Prosselkov, P.; Kongsuwan, K.; Epa, V. C.; Lilley, P. E.; Jergic, S.; Buchardt, J.; Brown, S. E.; Alewood, P. F.; Jennings, P. A.; Dixon, N. E. Inhibition of protein interactions with the β_2 sliding clamp of *Escherichia coli* DNA polymerase III by peptides derived from β_2-binding proteins. *Biochemistry.* **2004**, *43*, 5661–5671.

(17) Georgescu, R. E.; Kim, S. S.; Yurieva, O.; Kuriyan, J.; Kong, X. P.; O'Donnell, M. Structure of a sliding clamp on DNA. *Cell* **2008**, *132*, 43–54.

(18) Bunting, K. A.; Roe, S. M.; Pearl, L. H. Structural basis for recruitment of translesion DNA polymerase Pol IV/DinB to the β-clamp. *EMBO J* **2003**, *22*, 5883-5892.

(19) Yin, Z.; Kelso, M. J.; Beck, J. L.; Oakley, A. J. Structural and thermodynamic dissection of linear motif recognition by the *E. coli* sliding clamp. *J. Med. Chem.* **2013**, *56*, 8665–8673.

(20) Georgescu, R. E.; Yurieva, O.; Kim, S. S.; Kuriyan, J.; Kong, X. P.; O'Donnell, M. Structure of a small-molecule inhibitor of a DNA polymerase sliding clamp. *Proc. Natl. Acad. Sci. U.S.A.* **2008**, *105*, 11116–11121.

(21) Wijffels, G.; Johnson, W. M.; Oakley, A. J.; Turner, K.; Epa, V. C.; Briscoe, S. J.; Polley, M.; Liepa, A. J.; Hofmann, A.; Buchardt, J.; Christensen, C.; Prosselkov, P.; Dalrymple, B. P.; Alewood, P. F.; Jennings, P. A.; Dixon, N. E.; Winkler, D. A. Binding inhibitors of the bacterial sliding clamp by design. *J. Med. Chem.* **2011**, *54*, 4831–4838.

(22) Yin, Z.; Whittell, L. R.; Wang, Y.; Jergic, S.; Liu, M.; Harry, E. J.; Dixon, N. E.; Beck, J. L.; Kelso, M. J.; Oakley, A. J. Discovery of lead compounds targeting the bacterial sliding clamp using a fragment-based approach. *J Med Chem* **2014**, *57*, 2799–2806.

(23) Dohrmann, P. R.; McHenry, C. S. A bipartite polymerase-processivity factor interaction: only the internal β binding site of the α subunit is required for processive replication by the DNA polymerase III holoenzyme. *J. Mol. Biol.* **2005**, *350*, 228–239.

(24) Wolff, P.; Oliéric, V.; Briand, J. P.; Chaloin, O.; Dejaegere, A.; Dumas, P.; Ennifar, E.; Guichard, G.; Wagner, J.; Burnouf, D. Y. Structure-based design of short peptide ligands binding onto the *E. coli* processivity ring. *J. Med. Chem.* **2011**, *54*, 4627–4637.

(25) Kenakin, T. Radioligand binding experiments. In *Pharmacologic Analysis of Drug-Receptor Interaction*, 2nd ed.; Raven Press, 1993; pp. 385–410.

(26) Mortenson, P. N.; Murray, C. W. Assessing the lipophilicity of fragments and early hits. *J. Comput. Aided Mol. Des.* **2011**, *25*, 663–667.

(27) Berger, L.; Corraz, A. J.; Hoffmann-La Roche Inc.: 1977; Vol. US4009181 A.

(28) Napper, A. D.; Hixon, J.; McDonagh, T.; Keavey, K.; Pons, J.-F.; Barker, J.; Yau, W. T.; Amouzegh, P.; Flegg, A.; Hamelin, E.; Thomas, R. J.; Kates, M.; Jones, S.; Navia, M. A.; Saunders, J. O.; DiStefano, P. S.; Curtis, R. Discovery of indoles as potent and selective inhibitors of the deacetylase SIRT1. *J. Med. Chem.* **2005**, *48*, 8045–8054.

(29) Oakley, A. J.; Prosselkov, P.; Wijffels, G.; Beck, J. L.; Wilce, M. C.; Dixon, N. E. Flexibility revealed by the 1.85-Å crystal structure of the β sliding-clamp subunit of *Escherichia coli* DNA polymerase III. *Acta Crystallogr. D* **2003**, *59*, 1192–1199.

(30) Jergic, S.; Horan, N. P.; Elshenawy, M. M.; Mason, C. E.; Urathamakul, T.; Ozawa, K.; Robinson, A.; Goudsmits, J. M.H; Wang, Y.; Pan, X.; Beck, J. L.; van Oijen, A. M.; Huber, T.; Hamdan, S. M.; Dixon, N. E. A direct proofreader–clamp interaction stabilizes the Pol III replicase in the polymerization mode. *EMBO J.* **2013**, *32*, 1322–1333.

(31) Naktinis, V.; Onrust, R.; Fang, L.; O'Donnell, M. Assembly of a chromosomal replication machine: two DNA polymerases, a clamp loader, and sliding clamps in one holoenzyme particle. II. Intermediate complex between the clamp loader and its clamp. *J. Biol. Chem.* **1995**, *270*, 13358–13365.

(32) Leu, F. P.; O'Donnell, M. Interplay of clamp loader subunits in opening the β sliding clamp of *Escherichia coli* DNA polymerase III holoenzyme. *J. Biol. Chem.* **2001**, *276*, 47185–47194.

(33) Beck, J. L.; Urathamakul, T.; Watt, S. J.; Sheil, M. M.; Schaeffer, P. M.; Dixon, N. E. Proteomic dissection of DNA polymerization. *Expert Rev. Proteomics* **2006**, *3*, 197–211.

(34) Kelch, B. A.; Makino, D. L.; O'Donnell, M.; Kuriyan, J. How a DNA polymerase clamp loader opens a sliding clamp. *Science* **2011**, *334*, 1675–1680. *Science* **2011**, *334*, 1675-1680.

(35) Lacy, E. R.; Filippov, I.; Lewis, W. S.; Otieno, S.; Xiao, L.; Weiss, S.; Hengst, L.; Kriwacki, R. W. p27 binds cyclin-CDK complexes through a sequential mechanism involving binding-induced protein folding. *Nat Struct Mol Biol* **2004**, *11*, 358–364.

(36) Pawson, T.; Nash, P. Assembly of cell regulatory systems through protein interaction domains. *Science* **2003**, 300, 445–452.

(37) Tan, Z.; Wortman, M.; Dillehay, K. L.; Seibel, W. L.; Evelyn, C. R.; Smith, S. J.; Malkas, L. H.; Zheng, Y.; Lu, S.; Dong, Z. Small-molecule targeting of proliferating cell nuclear antigen chromatin association inhibits tumor cell growth. *Mol Pharmacol* **2012**, *81*, 811–819.

(38) Mason, C. E.; Jergic, S.; Lo, A. T.; Wang, Y.; Dixon, N. E.; Beck, J. L. *Escherichia coli* single-stranded DNA-binding protein: A nanoESI-MS study of salt-modulated subunit exchange and DNA binding transactions. *J. Am. Soc. Mass Spectrom.* **2013**, *24*, 274–285.

(39) Otwinowski, Z.; Minor, W. Processing of X-ray diffraction data collected in oscillation mode. *Methods Enzymol*. **1997**, *276*, 307–326.

(40) Winn, M. D.; Ballard, C. C.; Cowtan, K. D.; Dodson, E. J.; Emsley, P.; Evans, P. R.; Keegan, R. M.; Krissinel, E. B.; Leslie, A. G.; McCoy, A.; McNicholas, S. J.; Murshudov, G. N.; Pannu, N. S.; Potterton, E. A.; Powell, H. R.; Read, R. J.; Vagin, A.; Wilson, K. S. Overview of the CCP4 suite and current developments. *Acta Crystallogr. D* **2011**, *67*, 235–242.

(41) Emsley, P.; Cowtan, K. Coot: model-building tools for molecular graphics. *Acta Crystallogr. D* **2004**, *60*, 2126–2132.

(42) Skubak, P.; Murshudov, G. N.; Pannu, N. S. Direct incorporation of experimental phase information in model refinement. *Acta Crystallogr. D* **2004**, *60*, 2196–2201.

TOC figure

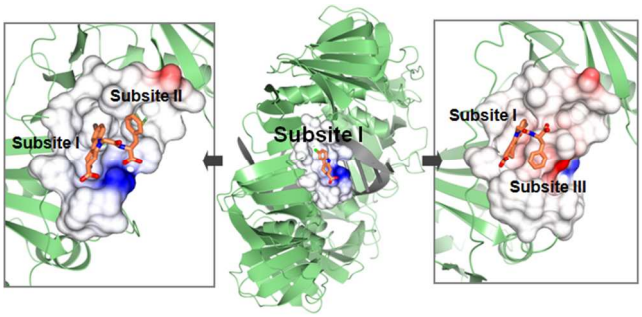

Bacterial Sliding Clamp Inhibitors that Mimic the Sequential Binding Mechanism of Endogenous Linear Motifs

Zhou Yin,[†,#] Louise R. Whittell,[†,#] Yao Wang,[†] Slobodan Jergic,[†] Cong Ma,[‡] Peter J. Lewis.[‡] Nicholas E. Dixon,[†] Jennifer L. Beck,[†] Michael J. Kelso,[†] and Aaron J. Oakley[,†]*

[†]School of Chemistry and Centre for Medical and Molecular Bioscience, The University of Wollongong, and The Illawarra Health and Medical Research Institute, Wollongong, New South Wales 2522, Australia

[‡]School of Environmental and Life Sciences, The University of Newcastle, Callaghan, New South Wales 2308, Australia

Supporting Information

Table of Contents

Supplementary Results

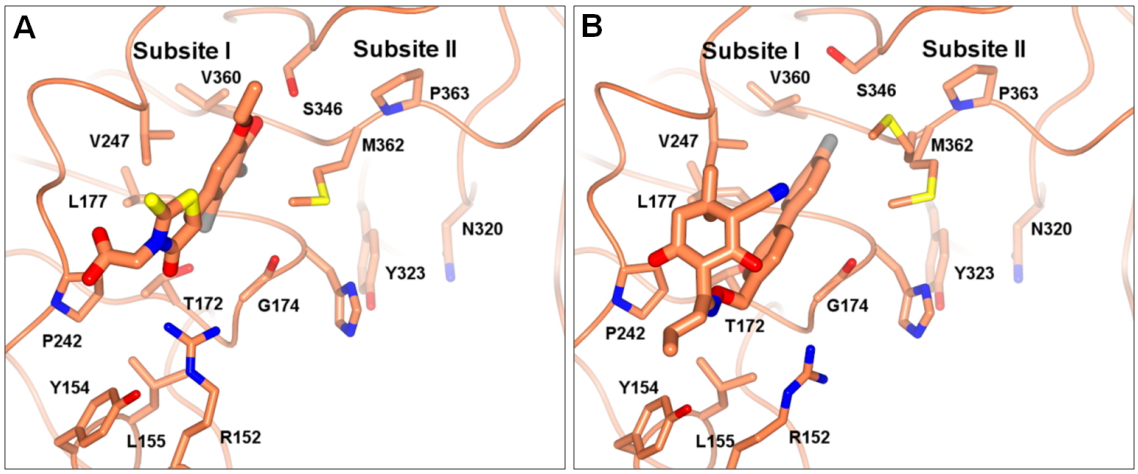

Figure S1. X-ray co-crystal structures of the *E. coli* SC in complex with (A) a thioxothiazolinine derivative (PDB entry 3D1G)[1] and (B) a biphenyloxime ether derivative (PDB entry 3QSB).[2] Carbon atoms are colored orange and non-carbon atoms follow CPK convention. Both inhibitors occupy subsite I.

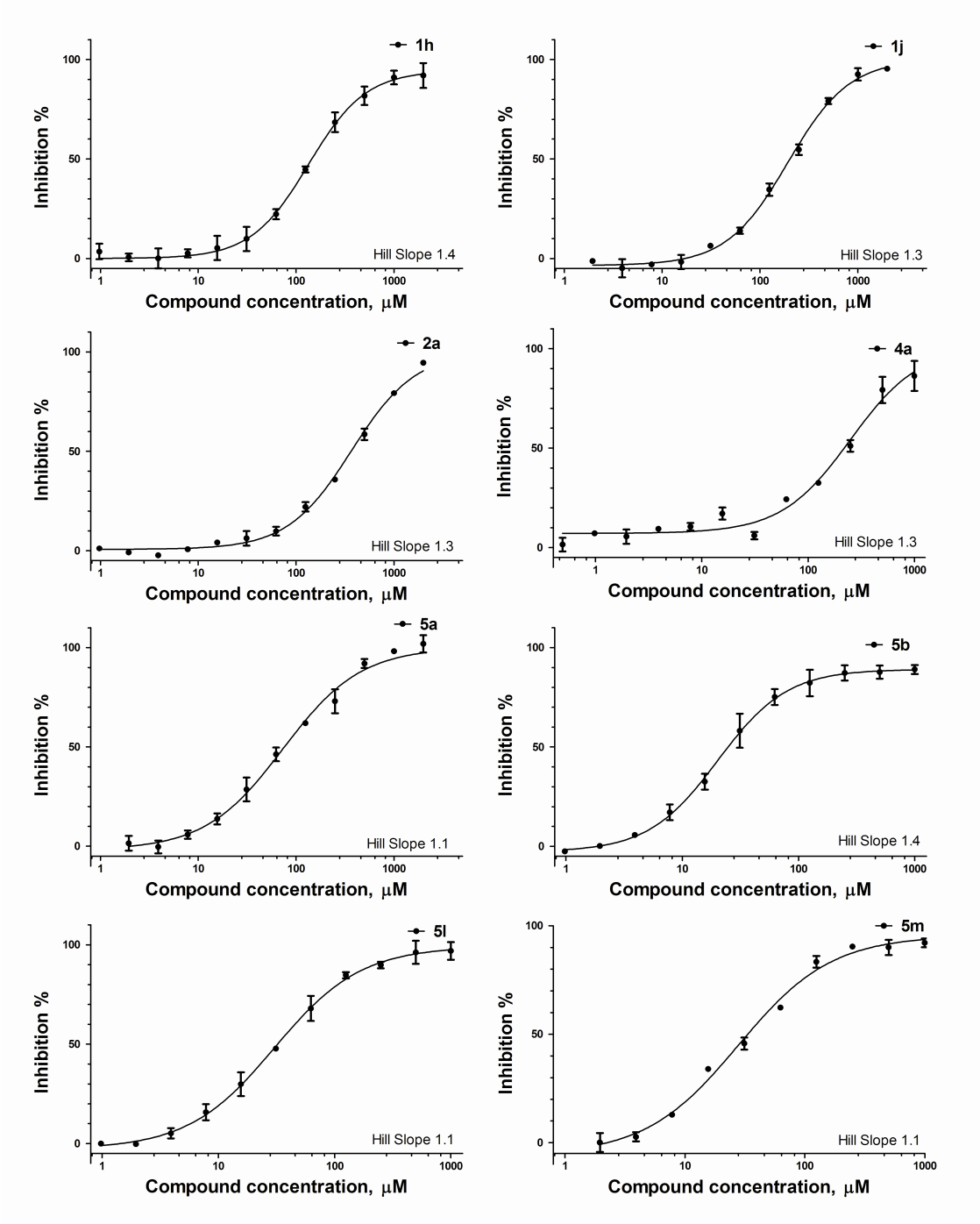

Figure S2. Dose-response curves of representative THC analogs inhibiting the *E. coli* SC, as measured by fluorescence polarization.

Table S1. Data collection and refinement statistics for X-ray co-crystal structures of the *E. coli* SC in complex with compounds 1e, 2a, 5b and 5l

Name	SC^{1e}	SC^{2a}	SC^{5b}	SC^{5l}
PDB Code	4OVF	4OVG	4OVH	4PNU
Data collection				
Space group	$P2_1$			
Cell dimensions	a, b, c (Å) / α, β, γ (°) 79.87, 67.26, 81.19 / 90.00, 114.27, 90.00	a, b, c (Å) / α, β, γ (°) 80.08, 66.20, 80.62 / 90.00, 114.89, 90.00	a, b, c (Å) / α, β, γ (°) 80.03, 66.42, 80.79 / 90.00, 114.76, 90.00	a, b, c (Å) / α, β, γ (°) 79.89, 67.19, 81.02 / 90.00, 114.54, 90.00
Resolution (Å)	50.00–2.05 (2.12–2.05)	40.00–1.90 (1.97–1.90)	30.00–2.25 (1.79–1.70)	30.00–1.90 (1.97–1.90)
R_{merge} (%)	4.3 (26.1)	2.8 (17.1)	7.1 (45.6)	3.2 (38.0)
No. of Reflections	169349	219352	116359	217379
Unique Reflections	49386 (4716)	60330 (6013)	37099 (3029)	61732 (5986)
Mean $I/\sigma(I)$	27.4 (3.5)	41.5 (7.0)	16.6 (2.2)	36.1 (2.7)
Completeness (%)	96.4 (95.9)	99.9 (100.0)	96.4 (82.4)	99.7 (97.4)
Multiplicity	3.6 (3.5)	3.7 (3.5)	3.1 (2.6)	3.5 (3.1)
Refinement				
Resolution (Å)	34.61–2.05 (2.10–2.05)	21.62–1.90 (1.95–1.90)	29.82–2.24 (2.29–2.24)	28.27–1.90 (1.95–1.90)
R_{work} / R_{free} (%)	21.0 (19.7) / 27.0 (29.9)	18.0 (21.9) / 22.6 (27.3)	19.2 (20.5) / 25.0 (32.1)	18.2 (25.0) / 23.0 (28.9)
RMS deviations				
Bond lengths (Å)	0.0056	0.0108	0.0070	0.0071
Bond angles (º)	1.0960	1.5211	1.2173	1.2654
B-factors				
main chain	22.6	17.1	24.8	17.8
sidechain & water	26.4	21.7	26.8	22.1
ligand*	32.7	22.1	33.1	20.3
Ramachandran Plot Outliers	0.43%	0.29%	0.42%	0.29%

Values for data in the highest resolution shell are given in parentheses.

Diffraction data were collected using a Rigaku 007HF X-ray generator producing Cu Kα X-rays (wavelength of 1.5418 Å) and Mar345dtb area detector. Diffraction data were processed using HKL2000.[3]

*Ligand refers to the compounds bound to SC chain A.

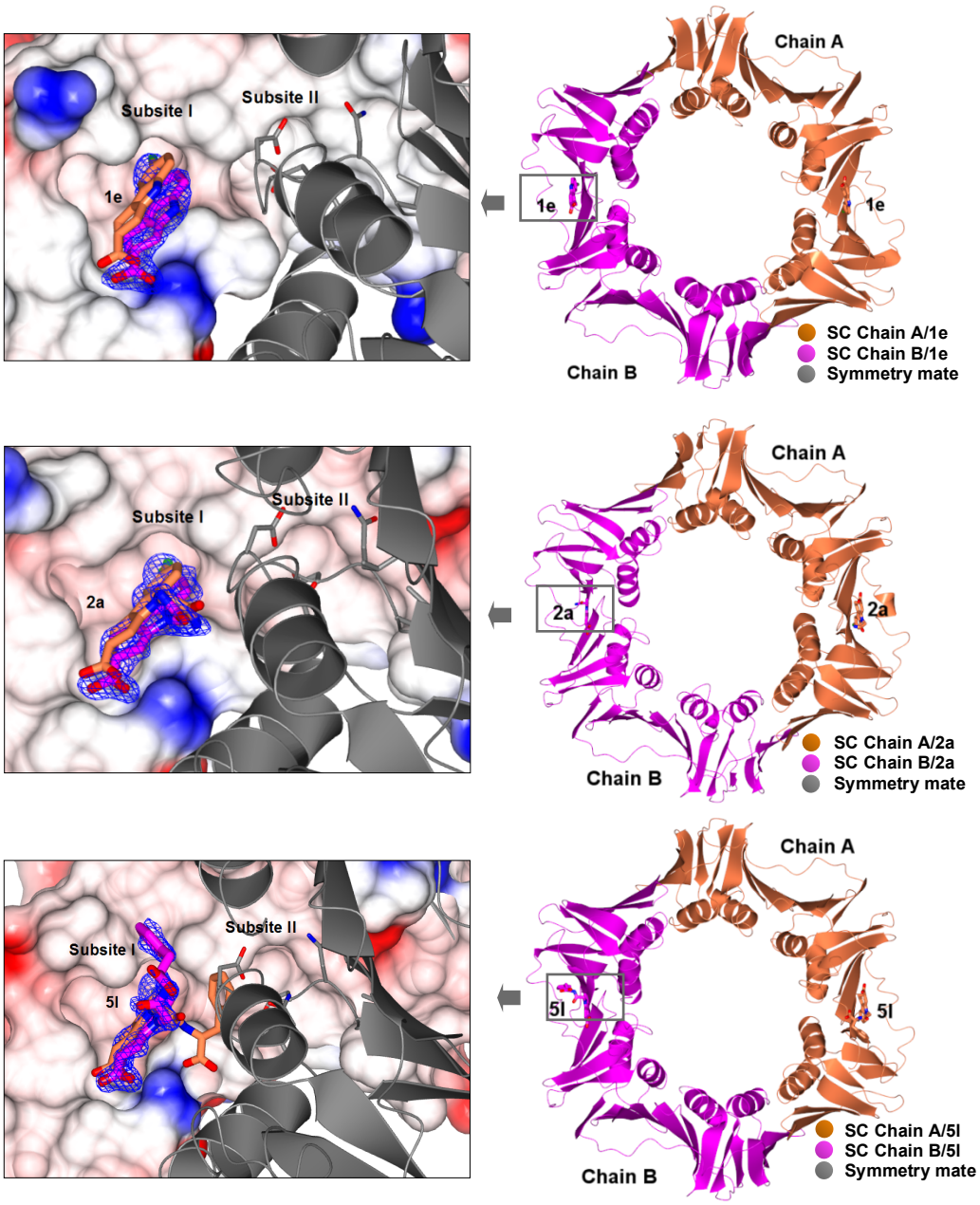

Figure S3. X-ray co-crystal structures of the *E. coli* SC showing chain B in complex with compounds **1e**, **2a** and **5l**. Carbon atoms of SC chain A/B and the bound compounds **1e**, **2a** and **5l** are colored orange/magenta respectively. All other atoms are colored according to the CPK convention. The SC symmetry partner is shown in gray. SC chain A is superimposed with chain B in the enlarged views and the electrostatic potential surfaces of chain B are shown with blue = positive and red = negative. Electron density maps ($2mF_o–DF_c$) contoured at 1σ are shown in blue wire-basket form.

Table S2. Data collection and refinement statistics for the X-ray crystal structures *of apo-E. coli* SC (SC^{apo}) and *E. coli* SC in complex with compound 5m (SC^{5m}), respectively

Structure Name	**SC^{apo}**	**SC^{5m}**
PDB Code	4PNV	4PNW
Data collection		
Space group	$P2_1$	
Cell dimensions	a, b, c (Å) / α, β, γ (°) 80.14, 70.26, 84.47 / 90.00, 114.67, 90.00	a, b, c (Å) / α, β, γ (°) 79.81, 68.71, 83.06 / 90.00, 115.72, 90.00
Resolution (Å)	30.00–1.86 (1.93–1.86)	30.00–2.00 (2.07–2.00)
R_{merge} (%)	2.8 (31.9)	5.1 (45.6)
No. of Reflections	251660	188410
Unique Reflections	71719 (6779)	55049 (5267)
Mean $I/\sigma(I)$	41.1 (3.2)	24.0 (2.6)
Completeness (%)	99.3 (95.3)	98.0 (96.2)
Multiplicity	3.5 (3.1)	3.4 (3.2)
Refinement		
Resolution (Å)	27.55–1.86 (1.91–1.86)	28.01–2.00 (2.05–2.00)
R_{work} / R_{free} (%)	18.3(26.0) / 23.3(33.8)	18.4(20.4) / 23.3(28.2)
R.M.S. deviations		
Bond lengths (Å)	0.0067	0.0079
Bond angles (°)	1.2017	1.3198
B-factors		
mainchain	19.4	23.1
sidechain & water	23.8	26.8
ligand*	N/a	39.4
Ramachandran Plot Outliers	0.29%	0.57 %

Values for data in the highest resolution shell are given in parentheses.

Diffraction data were collected using a Rigaku 007HF X-ray generator producing Cu Kα X-rays (wavelength of 1.5418 Å) and Mar345dtb area detector. Diffraction data were processed with HKL2000.[3]

*Ligand refers to compounds bound to SC Chain B.

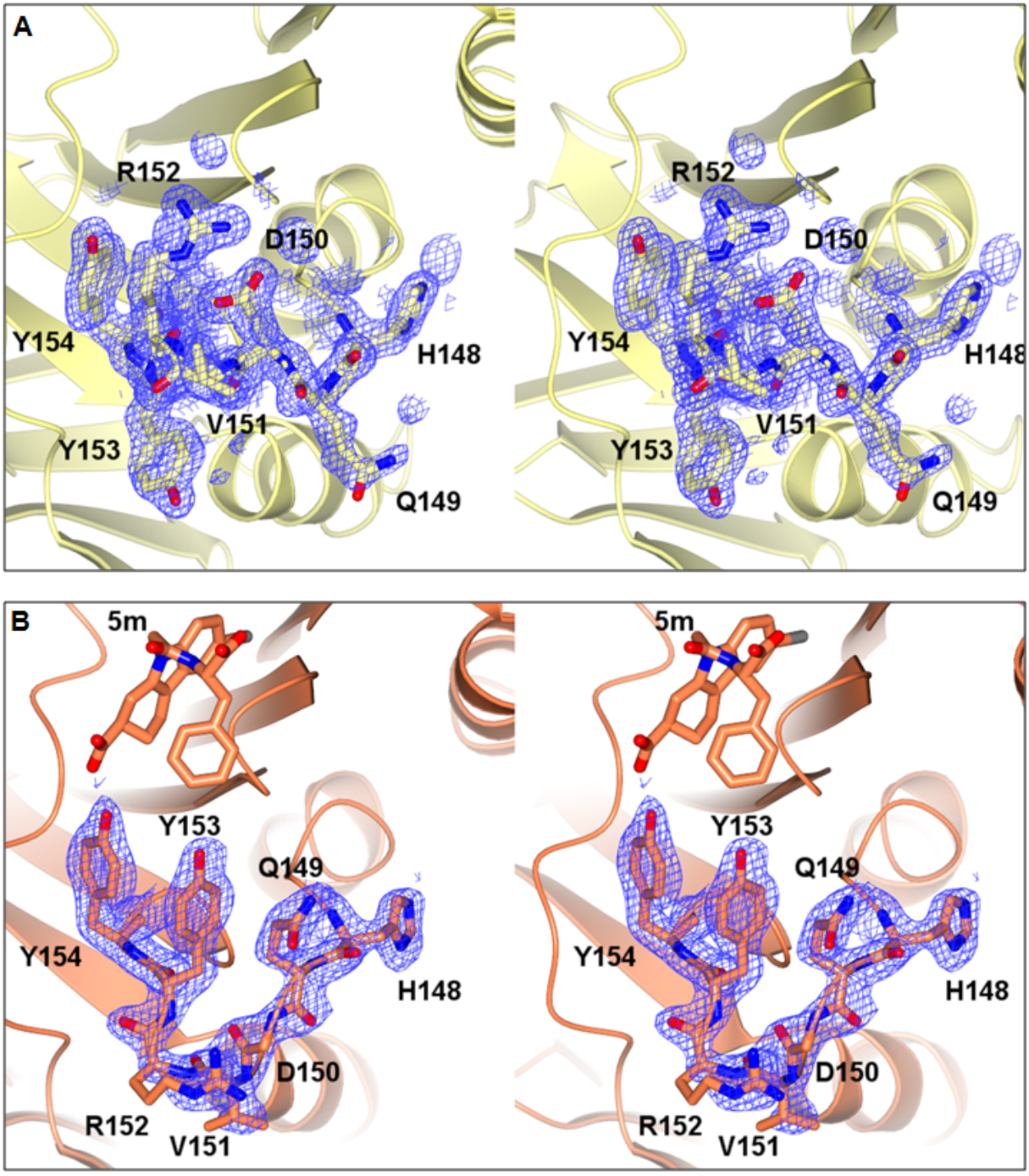

Figure S4. Stereo view of the loop rearrangement induced upon binding of compound **5m** to the *E. coli* SC. (A) The H148–Y154 loop region of SC^{apo}. Carbon atoms are shown in yellow. All other atoms are colored according to CPK convention. (B) The H148–Y154 loop region of $SC^{\mathbf{5m}}$. Carbon atoms are colored orange. All other atoms are colored according to CPK convention. Electron density maps ($2mF_o–DF_c$) contoured at 1σ are shown in blue wire-basket form.

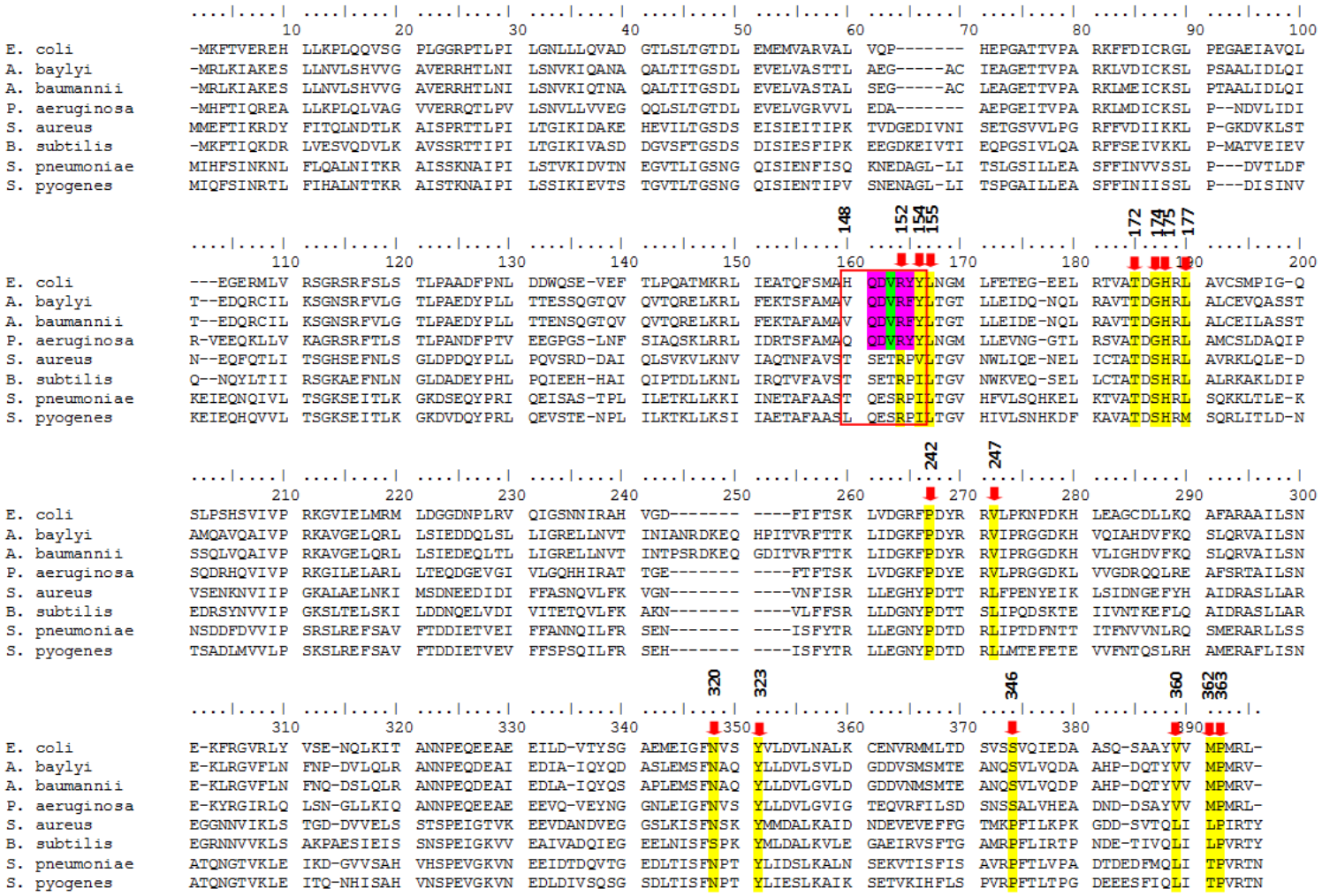

Figure S5. Sequence Alignment of SCs from four representative Gram-negative (*Escherichia coli*, *Acinetobacter baylyi*, *Acinetobacter baumannii* and *Pseudomonas aeruginosa*) and four Gram-positive bacterial species (*Staphylococcus aureus*, *Bacillus subtilis*, *Streptococcus pneumoniae* and *Streptococcus pyogenes*). Red box indicates the H148–Y154 loop region. The switching pairs of residues, i.e., Q149–D150 and R152–Y153, are highlighted in purple and V151 in green for the Gram-negative species. Residues comprising subsites I and II are highlighted in yellow. Numbering is based on the *E. coli* SC sequence.

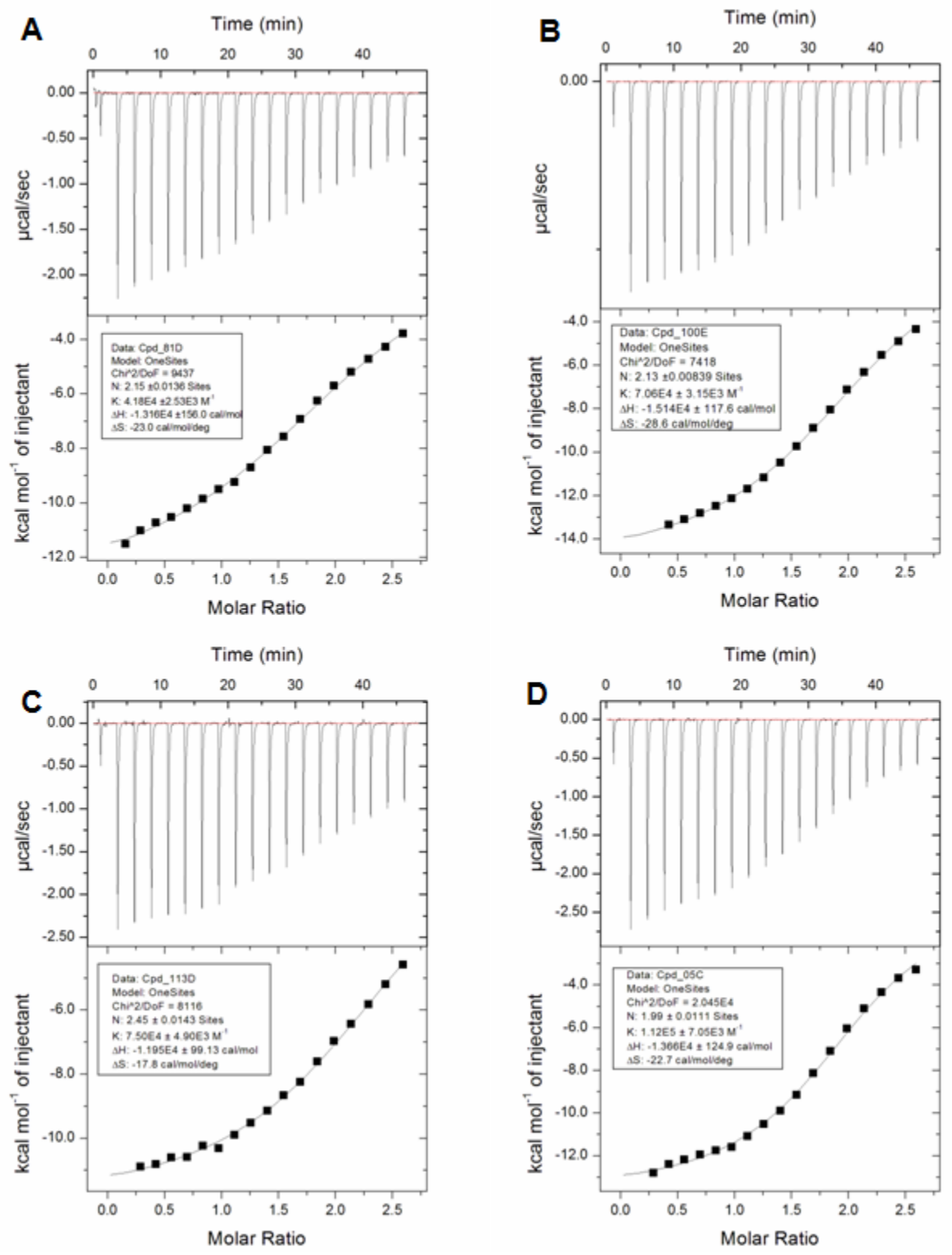

Figure S6. Isothermal titration calorimetry data for the binding of (A) **5a**, (B) **5b**, (C) **5l** and (D) **5m** to the *E. coli* SC.

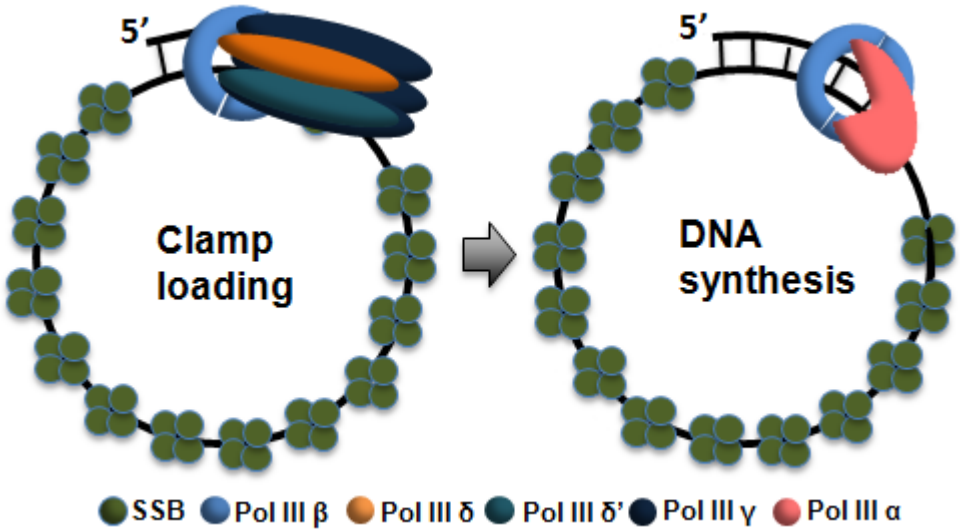

Figure S7. Schematic representation of the *in vitro* DNA replication assay.

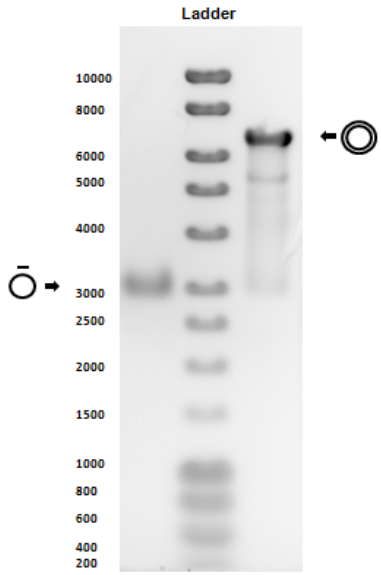

Figure S8. Control *in vitro* DNA replication assay. Molecular sizes (in bp) corresponding to bands in the DNA ladder are shown. The circle with dashed line above represents primed ssDNA template. Two concentric circles represent completed dsDNA replication products.

Supplementary Methods

Chemo-informatics. LogD values at *p*H 7.2 were calculated using Accord for Excel 6.2 (Accelrys). Calculations of Ligand Lipophilicity Efficiency (LLE_{AT}) followed the published methods[4] and are summarized below:

$\Delta G^* = \Delta G - \Delta G_{lipo}$

$= RT\ln(K_i) + RT\text{LogD}$

$LLE_{AT} = 0.11 - \Delta G^*/HAC$

ΔG: difference in Gibbs free energy; K_i: inhibition constant; HAC: heavy atom count; LogD: distribution coefficient at *p*H 7.2.

Bioinformatics. Sequence alignments of bacterial sliding clamps (NCBI IDs: YP_859300.1, WP_004930066.1, ZP_08441263.1, NP_064722.1, NP_373240.1, WP_003242509.1, YP_815419.1 and AAF98349.2) were carried out with COBALT.[5]

Chemistry – General. ^{1}H and ^{13}C NMR spectra were acquired on a Varian Mercury 300 MHz, Varian Inova 500 MHz or VNMRS 500 MHz spectrometer. Chemical shifts (δ) are reported in ppm relative to the solvent and coupling constants (*J*) are in Hz. Electrospray ionisation (EI) low resolution mass spectra (LRMS) were recorded on a Waters Micromass Platform LCZ spectrometer. High resolution mass spectra (HRMS) were recorded on a Waters Xevo spectrometer using either an EI source or atmospheric solids analysis probe (ASAP). Melting points were recorded using a Gallenkamp (Griffin) melting point apparatus and are uncorrected. Optical rotations were measured on a Jasco P-2000 polarimeter. TLC analysis was performed using pre-coated Merck silica gel 60 PF_{254} aluminium sheets. Flash column chromatography was performed using Davisil silica gel (40-63 μm). Petrol refers to petroleum spirits of bp 40–60°C. All compounds examined showed ≥ 95% purity by ^{1}H NMR and HPLC-MS.

(±)-6-Chloro-2,3,4,9-tetrahydrocarbazole-2-carboxylic acid (1a).[6,7] To a solution of 4-chlorophenylhydrazine hydrochloride (305 mg, 1.70 mmol) in glacial acetic acid (2 mL) was added 3-oxo-cyclohexanecarboxylic acid (237 mg, 1.67 mmol) in glacial acetic acid (2 mL) and the mixture heated at reflux overnight. The reaction mixture was cooled and the resulting precipitate collected by vacuum filtration and washed with cold water. The resultant solid was purified by silica gel column chromatography (25:75:0.5 to 50:50:0.5 Et_2O/petrol/AcOH) followed by recrystallization from EtOH/H_2O to give **1a** (42 mg, 10% yield) as a yellow powder: mp 242–244°C (lit.[6] 249–250°C); ^{1}H NMR (DMSO-d_6, 500 MHz): δ 1.80–183 (1H, m), 2.14–2.16 (1H, m), 2.56–2.92 (5H, m), 6.97 (1H, d, *J* = 8.0 Hz), 7.24 (1H, d, *J* = 8.5 Hz), 7.34 (1H, s), 10.90 (1H, s), 12.32 (1H, s.); ^{13}C NMR (DMSO-d_6, 125 MHz): δ 19.4, 25.1, 25.7, 39.3, 107.6, 112.0, 116.5, 119.9, 122.8, 128.1, 134.3, 135.2, 175.97; LRMS (ES^+) *m/z*: 272.2 $[M+Na]^+$; HRMS ($ASAP^+$) calcd. for $C_{13}H_{13}NO_2Cl$ $[M+H]^+$ 250.0635, found 250.0628.

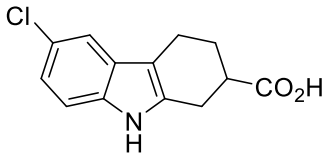

(±)-Methyl 6-chloro-2,3,4,9-tetrahydro-1H-carbazole-2-carboxylate (1b).[6] To a solution of **1a** (50 mg, 0.20 mmol) in MeOH (1.5 mL) was added concentrated H_2SO_4 (200 μL) and the mixture heated at reflux overnight. The resulting solution was cooled, concentrated to dryness, treated with saturated aqueous $NaHCO_3$ and extracted with EtOAc (3 x 10 mL). The combined organic extracts were

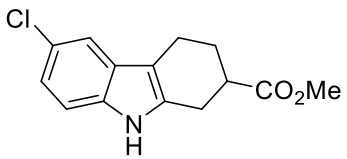

washed with water (10 mL) and brine (10 mL), dried over anhydrous $MgSO_4$ and concentrated. The crude residue was recrystallized from MeOH/H_2O to give **1b** (16 mg, 31% yield) as a beige powder: mp 164–166 °C (lit.[6] 175–176 °C); ^{1}H NMR (DMSO-d_6, 500 MHz): δ 1.81–1.86 (1H, m), 2.15–2.17 (1H, m), 2.59–2.71 (2H, m), 2.89–2.96 (3H, m), 3.65 (3H, s), 6.98 (1H, dd, *J* = 18.5, 2.0 Hz), 7.26 (1H, d, *J* = 9.0 Hz), 7.35 (1H, d, *J* = 1.0 Hz), 10.94 (1H, brs); ^{13}C NMR (DMSO-d_6, 125 MHz): δ 19.4, 25.1, 25.7, 39.1, 51.6, 107.6, 112.0, 116.6, 120.0, 122.8, 128.0, 134.3, 134.8, 174.7; LRMS (ES^+) *m/z*: 264.1 $[M+H]^+$; HRMS (ES^+) calcd. for $C_{14}H_{15}NO_2Cl$ $[M+H]^+$ 264.0791, found 264.0791.

(±)-6-Chloro-2,3,4,9-tetrahydro-1H-carbazole-2-carboxamide (1c).[7] To a solution of **1a** (75 mg, 0.30 mmol) in dry CH_2Cl_2 (2 mL) containing a few drops of DMF was added *N*-hydroxysuccinimide (59 mg, 0.51 mmol) and *N*-(3-dimethylaminopropyl)-*N*′-ethylcarbodiimide hydrochloride (97 mg, 0.51 mmol) and the mixture stirred for 2.5 h at room temperature. The resulting suspension was diluted with water and extracted with CH_2Cl_2 (3 x 10 mL). The combined organic extracts were dried over anhydrous $MgSO_4$ and concentrated. The resultant residue was redissolved in THF (1 mL), NH_4OH (28%; 1 mL) added and the mixture stirred for 2 h. The resulting orange solution was diluted with water and extracted with EtOAc (3 x 20 mL). The combined organic extracts were washed with brine (10 mL), dried over anhydrous $MgSO_4$ and concentrated. Trituration of the residue with CH_2Cl_2 gave **1c** (23 mg, 31% yield) as an off-white powder: mp 194–196°C (lit.[6] 203–204 °C); ^{1}H NMR (DMSO-d_6, 500 MHz): δ 1.69–1.75 (1H, m), 2.05–2.09 (1H, m), 2.53–2.64 (2H, m), 2.71–2.87 (3H, m), 6.87 (1H, br s), 6.97 (1H, dd, *J* = 8.0, 1.3 Hz), 7.24 (1H, d, *J* = 8.5 Hz), 7.35 (1H, s), 7.42 (1H, br s), 10.90 (1H, s); ^{13}C NMR (DMSO-d_6, 125 MHz): δ 19.9, 25.5, 26.7, 40.4, 107.6, 112.0, 116.5, 119.9, 122.8, 128.1, 134.3, 135.7, 176.5; LRMS (ES^+) *m/z*: 271.11 $[M+Na]^+$; HRMS (ES^+) calcd. for $C_{13}H_{13}N_2OClNa$ $[M+Na]^+$ 271.0614, found 271.0616.

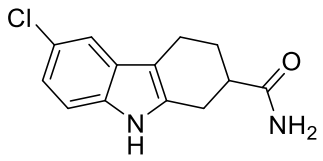

(±)-(6-Chloro-2,3,4,9-tetrahydro-1H-carbazol-2-yl)methanol (1d).[6] To a solution of **1a** (75 mg, 0.30 mmol) in dry THF (2 mL) was added portion-wise $LiAlH_4$ (35 mg, 0.93 mmol) and the mixture stirred at room temperature for 3 h. A saturated solution of sodium potassium tartrate in water was then added and the mixture stirred for 30 min before being extracted with EtOAc (3 x 20 mL). The combined organic extracts were washed with brine (10 mL), dried over anhydrous $MgSO_4$ and concentrated. The resulting residue was triturated with CH_2Cl_2 to give **1d** (30 mg, 20% yield) as a yellow powder: mp 152–154°C (lit.[6] 168–169 °C); ^{1}H NMR (CD_3OD, 500 MHz): δ 1.50–1.52 (1H, m), 2.04–2.05 (2H, m), 2.43–2.48 (1H, m), 2.59–2.61 (1H, m), 2.71–2.74 (1H, m), 2.81–2.85 (1H, m), 3.55–3.62 (2H, m), 6.94 (1H, d, *J* = 8.0 Hz), 7.17 (1H, d, *J* = 8.5 Hz), 7.29 (1H, s); ^{13}C NMR (CD_3OD, 125 MHz): δ 21.0, 27.2, 27.4, 38.4, 67.5, 109.8, 112.4, 117.6, 121.2, 125.0, 130.0, 136.2, 136.8; LRMS (ES^+) *m/z*: 258.0 $[M+Na]^+$; HRMS (ES^+) calcd. for $C_{13}H_{13}NO_2Cl$ $[M+H]^+$ 236.0842, found 236.0831.

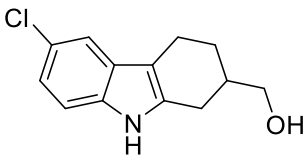

(*R*)-6-Chloro-2,3,4,9-tetrahydro-1H-carbazole-2-carboxylic acid (1e). To a solution of (*R*)-3-oxo-cyclohexane-1-carboxylic acid (104 mg, 0.12 mmol) in glacial acetic acid (0.5 mL), 4-chlorophenylhydrazine hydrochloride (136 mg, 0.76 mmol) was added in glacial acetic acid (1.0 mL) and the resulting suspension heated at reflux overnight. The reaction mixture was cooled, diluted with water (15 mL) and extracted with EtOAc (3 x 15 mL). The combined organic extracts were washed with water (10 mL), brine (10 mL), dried over anhydrous $MgSO_4$ and concentrated. The resulting residue was purified by silica gel column chromatography (20:80:0.5 to 50:50:0.5 Et_2O/petrol/acetic acid) followed by trituration with petrol to give **1e** (31 mg, 17% yield) as a yellow crystalline solid: mp 242–244°C (lit.[6] 249–251°C); ^{1}H NMR (CD_3OD, 500 MHz): δ 1.86–1.94 (1H, m),

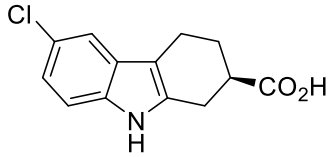

2.25–2.27 (1H, m), 2.60–2.66 (1H, m), 2.73–2.78 (1H, m), 2.80–2.86 (1H, m), 2.91 (2H, br d, *J* = 7.5 Hz), 6.95 (1H, dd, *J* = 8.5, 1.8 Hz), 7.17 (1H, d, *J* = 8.5 Hz), 7.29 (1H, s), 10.2 (1H, br s); ^{13}C NMR (CD_3OD, 125 MHz): δ 20.9, 26.5, 27.5, 41.3, 109.2, 112.5, 117.7, 121.5, 125.1, 129.8, 135.7, 136.2, 178.9; LRMS (ES^-) *m/z*: 248.0 $[M-H]^-$; HRMS (ES^-) calcd. for $C_{13}H_{11}NO_2Cl$ $[M-H]^-$ 248.0478, found 248.0486; $[\alpha]_{589}^{25}$ +47.7 (c 1.02, MeOH).

(*S*)-6-Chloro-2,3,4,9-tetrahydro-1H-carbazole-2-carboxylic acid (1f). The compound was prepared according to the method described for **1e** from (*S*)-3-oxo-cyclohexane-1-carboxylic acid (101 mg, 0.71 mmol) and 4-chlorophenylhydrazine hydrochloride (133.0 mg, 0.74mmol). **1f** (59 mg, 33% yield) was obtained as a yellow crystalline solid: mp 244–246°C (lit[6] 249–250°C); ^{1}H NMR (CD_3OD, 500 MHz): δ 1.87–1.95 (1H, m), 2.25–2.28 (1H, m), 2.61–2.67 (1H, m), 2.74–2.79 (1H. m), 2.81–2.86 (1H, m), 2.95 (2H, d, *J* = 7.0Hz), 6.95 (1H, dd, *J* = 8.5, 1.5 Hz), 7.17 (1H, d, *J* = 9.0 Hz), 7.29 (1H, d, *J* = 1.5 Hz), 10.19 (1H, br s); ^{13}C NMR (CD_3OD, 125 MHz): δ 20.9, 26.6, 27.5, 41.4, 109.3, 112.6, 117.7, 121.5, 125.2, 129.8, 135.8, 136.3, 178.9; LRMS (ES^+) *m/z*: 250.0 $[M+H]^+$; HRMS ($ASAP^+$) calcd. for $C_{13}H_{13}NO_2Cl$ $[M+H]^+$ 250.0635, found 250.0643; $[\alpha]_{589}^{25}$ –45.2 (c 1.02, MeOH).

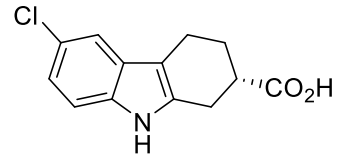

(*R*)-6-Fluoro-2,3,4,9-tetrahydro-1H-carbazole-2-carboxylic acid (1g). The compound was prepared according to the method described for **1e** from (*R*)-3-oxo-cyclohexane-1-carboxylic acid (127 mg, 0.89 mmol) and 4-fluorophenylhydrazine hydrochloride (122 mg, 0.75 mmol). **1g** (51 mg, 29% yield) was obtained as a yellow powder: mp 244–246°C; ^{1}H NMR (CD_3OD, 300 MHz): δ 1.87–1.96 (1H, m), 2.24–2.28 (1H, m), 2.58–2.86 (3H, m), 2.95 (2H, d, *J* = 7.2 Hz), 6.75 (1H, t, *J* = 9.0 Hz), 6.98 (1H, d, *J* = 9.9 Hz), 7.14–7.18 (1H, m), 10.09 (1H, br s); ^{13}C NMR (CD_3OD, 75 MHz): δ 21.0, 26.6, 27.6, 41.4, 103.1 (d, *J* = 24.0 Hz), 109.1 (d, *J* = 26.3 Hz), 109.5 (d, *J* = 4.6 Hz), 112.0 (d, *J* = 10.3 Hz), 128.9 (d, *J* = 10.3 Hz), 134.3, 136.0, 158.8 (d, *J* = 230.0 Hz), 179.0; LRMS (ES^-) *m/z*: 232.0 $[M-H]^-$; HRMS (ES^-) calcd. for $C_{13}H_{11}NO_2F$ $[M-H]^-$ 232.0774, found 232.0769; $[\alpha]_{589}^{25}$ +16.2 (c 0.52, MeOH).

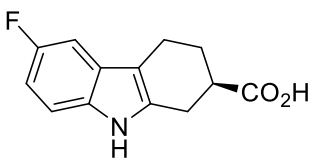

(*R*)-6-Iodo-2,3,4,9-tetrahydro-1H-carbazole-2-carboxylic acid (1h). The compound was prepared according to the method described for **1e** from (*R*)-3-oxo-cyclohexane-1-carboxylic acid (84 mg, 0.59 mmol) and 4-iodophenylhydrazine (107 mg, 0.46 mmol). **1h** (24 mg, 15% yield) was obtained as a brown powder: mp 202–204°C; ^{1}H NMR (CD_3OD, 500 MHz): δ 1.88–1.95 (1H, m), 2.25–2.28 (1H, m), 2.60–2.67 (1H, m), 2.73–277 (1H, m), 2.81–2.86 (1H, m), 2.95 (2H, d, *J* = 7.0 Hz), 7.05 (1H, d, *J* = 9.0 Hz), 7.25 (1H, d, *J* = 8.0 Hz), 7.65 (1H, s), 10.22 (1H, br s); ^{13}C NMR (CD_3OD, 125 MHz): δ 20.9, 26.5, 27.5, 41.4, 82.2, 108.8, 113.6, 127.3, 129.8, 131.3, 135.2, 136.9, 178.9; LRMS (ES^-) *m/z*: 340.0 $[M-H]^-$; HRMS (ES^-) calcd. for $C_{13}H_{11}NO_2I$ $[M-H]^-$ 339.9835, found 339.9830; $[\alpha]_{589}^{25}$ –27.7 (c 0.28, MeOH).

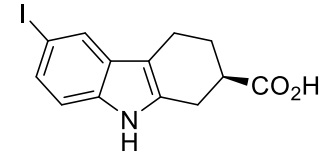

(*R*)-6-Bromo-2,3,4,9-tetrahydro-1H-carbazole-2-carboxylic acid (1i). The compound was prepared according to the method described for **1e** from (*R*)-3-oxo-cyclohexane-1-carboxylic acid (568 mg, 3.99 mmol) and 4-bromophenylhydrazine hydrochloride (908 mg, 4.06 mmol). **1i** (943 mg, 80% yield) was obtained as a yellow powder: mp 230–232°C;^{1}H NMR (CD_3OD, 500 MHz): δ 1.87–1.95 (1H, m), 2.25–2.28 (1H, m), 2.61–2.67 (1H, m), 2.74–2.87 (2H, m), 2.96 (2H, d, *J* =

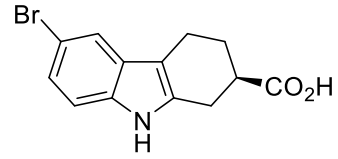

7.0 Hz), 7.08 (1H, d, *J* = 8.5 Hz), 7.14 (1H, d, *J* = 8.5 Hz), 7.45 (1H, s); ^{13}C NMR (CD_3OD, 125 MHz): δ 20.9, 26.5, 27.5, 41.4, 109.1, 112.6, 113.0, 120.9, 124.1, 130.5, 135.6, 136.4, 178.9; LRMS (ES^-) *m/z*: 294.0 $[M-H]^-$; HRMS (ES^-) calcd. for $C_{13}H_{11}NO_2Br$ $[M-H]^-$ 291.9973, found 291.9964; $[\alpha]_{589}^{25}$+49.0 (c 0.51, MeOH).

(*S*)-6-Bromo-2,3,4,9-tetrahydro-1H-carbazole-2-carboxylic acid (1j). The compound was prepared according to the method described for **1e** from (*S*)-3-oxo-cyclohexane-1-carboxylic acid (241 mg, 1.70 mmol) and 4-bromophenylhydrazine hydrochloride (405 mg, 1.81 mmol). **1j** (212 mg, 42% yield) was obtained as a yellow powder: mp 236–238°C; ^{1}H NMR (CD_3OD, 500 MHz): δ 1.89–1.90 (1H, m), 2.24 –2.26 (1H, m), 2.61–2.67 (1H, m), 2.72–2.95 (4H, m), 7.07 (1H, br d, *J* = 8.0 Hz), 7.13 (1H, d, *J* = 7.5 Hz), 7.44 (1H, s); ^{13}C NMR (CD_3OD, 125MHz): δ 20.9, 26.5, 27.5, 41.4, 109.1, 112.5, 113.0, 120.9, 124.1, 130.4, 135.6, 136.4, 178.9; LRMS (ES^-) *m/z*: 292.0 $[M-H]^-$; HRMS (ES^-) calcd. for $C_{13}H_{11}NO_2Br$ $[M-H]^-$ 291.9973, found 291.9980; $[\alpha]_{589}^{25}$ –39.6 (c 0.52, MeOH).

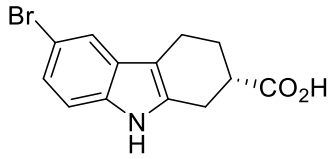

Ethyl (*R*)-6-chloro-2,3,4,9-tetrahydro-1H-carbazole-2-carboxylate (1k). To a solution of 4-chlorophenylhydrazine hydrochloride (974 mg, 6.85 mmol) in glacial acetic acid (8 mL) was added (*R*)-3-oxo-1-cyclohexane carboxylic acid (702 mg, 4.94 mmol) and the suspension heated at reflux for 6 h. The reaction mixture was cooled, diluted with water and extracted with EtOAc (3 x 50 mL). The combined organic extracts were washed with water (50 mL), brine (50 mL), dried over anhydrous $MgSO_4$ and concentrated. The resulting crude residue was redissolved in absolute ethanol (5 mL) containing concentrated H_2SO_4 (100 µL) and the reaction heated at reflux overnight. The solution was cooled, concentrated, made alkaline with saturated $NaHCO_{3(aq)}$ and the mixture extracted with EtOAc (3 x 40 mL). The combined organic fractions were washed with brine (40 mL), dried over anhydrous $MgSO_4$ and concentrated. The resulting residue was purified by silica gel column chromatography (10:0–8:2 Et_2O/petrol) to give **1k** (877 mg, 64% yield) as a yellow powder: mp 130–132°C; ^{1}H NMR ($CDCl_3$, 500 MHz): δ 1.29 (3H, t, *J* = 7.3 Hz), 1.91–1.98 (1H, m), 2.28–2.31 (1H, m), 2.64–2.70 (1H, m), 2.77–3.05 (4H, m), 4.16–4.21 (2H, m), 7.06 (1H, d, *J* = 8.0 Hz), 7.16 (1H, d, *J* = 8.5 Hz), 7.39 (1H, s), 7.83 (1H, br s); ^{13}C NMR ($CDCl_3$, 125 MHz): δ 14.4, 20.1, 25.7, 26.3, 40.3, 60.9, 109.5, 111.5, 117.6, 121.5, 125.1, 128.6, 134.0, 134.4, 175.1; LRMS (ES^+) *m/z*: 278.0 $[M+H]^+$; HRMS (ES^+) calcd. for $C_{15}H_{17}NO_2Cl$ $[M+H]^+$ 278.0948, found 278.0938; $[\alpha]_{589}^{25}$ +48.4 (c 1.05, MeOH).

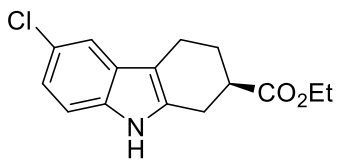

Ethyl (*S*)-6-chloro-2,3,4,9-tetrahydro-1H-carbazole-2-carboxylate (1l). The compound was prepared according to the method described for **1k** from (*S*)-3-oxocyclohexane-1-carboxylic acid (272 mg, 1.91 mmol) and 4-chlorophenylhydrazine hydrochloride (340 mg, 1.89 mmol). **1l** was obtained (184 mg, 35% yield) as a pale yellow solid: mp 130–132°C; ^{1}H NMR ($CDCl_3$, 500 MHz): δ 1.29 (3H, t, *J* = 7.3 Hz), 1.92–1.98 (1H, m), 2.29–2.31 (1H, m), 2.65–2.71 (1H, m), 2.77–3.05 (4H, m), 4.17–4.23 (2H, m), 7.06 (1H, dd, *J* = 8.0, 1.5 Hz), 7.17 (1H, d, *J* = 9.0 Hz), 7.40 (1H, s), 7.81 (1H, br s); ^{13}C NMR ($CDCl_3$, 125 MHz): δ 14.4, 20.1, 25.7, 26.3, 40.3, 60.9, 109.5, 111.5, 117.6, 121.6, 125.1, 128.6, 134.0, 134.4, 175.1; LRMS (ES^-) *m/z*: 276.0 $[M-H]^-$; HRMS (ES^-) calcd. for $C_{15}H_{15}NO_2Cl$ $[M-H]^-$ 276.0791, found 276.0780; $[\alpha]_{589}^{25}$ –42.8 (c 1.03, MeOH).

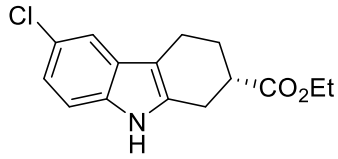

Ethyl (*R*)-6-bromo-2,3,4,9-tetrahydro-1H-carbazole-2-carboxylate (1m). The compound was prepared according to the method described for **1k** from (*R*)-3-oxocyclohexane-1-carboxylic acid (2.28 g, 10.18

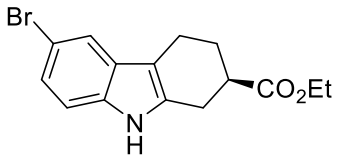

mmol) and 4-bromophenylhydrazine hydrochloride (1.45 g, 10.17 mmol). **1m** (1.99 g, 58% yield) was obtained as a yellow powder: mp 144–146°C; ^{1}H NMR ($CDCl_3$, 500 MHz): δ 1.29 (3H, t, *J* = 7.0 Hz), 1.92–1.98 (1H, m), 2.28–2.31 (1H, m), 2.65–2.70 (1H, m), 2.77–3.05 (4H, m), 4.17–4.23 (2H, m, CH_2), 7.11 (1H, d, *J* = 8.5 Hz), 7.18 (1H, d, *J* = 8.5 Hz), 7.55 (1H, s), 7.84 (1H, br s); ^{13}C NMR ($CDCl_3$, 125 MHz): δ 14.5, 20.1, 25.7, 26.4, 40.3, 61.0, 109.5, 112.1, 112.7, 120.7, 124.2, 129.3, 133.9, 134.8, 175.2; LRMS (ES^+) *m/z*: 362.0 $[M+K]^+$; HRMS (ES^+) calcd. for $C_{15}H_{17}NO_2Br$ $[M+H]^+$ 322.0443, found 322.0443; $[\alpha]_{589}^{25}$ +49.5 (c 1.04, MeOH).

Ethyl (*S*)-6-bromo-2,3,4,9-tetrahydro-1H-carbazole-2-carboxylate (1n). The compound was prepared according to the method described for **1k** from (*S*)-3-oxocyclohexane-1-carboxylic acid (227 mg, 1.60 mmol) and 4-bromophenylhydrazine hydrochloride (387 mg, 1.73 mmol). **1n** (183 mg, 35% yield) was obtained as a yellow powder: mp 136–138°C; ^{1}H NMR ($CDCl_3$, 500 MHz): δ 1.29 (3H, d, *J* = 7.3 Hz), 1.90–1.98 (1H, m), 2.28–2.31 (1H, m), 2.64–2.70 (1H, m), 2.76–3.04 (4H, m), 4.16–4.23 (2H, m, CH_2), 7.11 (1H, d, *J* = 8.5 Hz), 7.18 (1H, dd, *J* = 8.0, 1.5 Hz), 7.55 (1H, s), 7.84 (1H, br s); ^{13}C NMR ($CDCl_3$, 125 MHz): δ 14.4, 20.1, 25.6, 26.3, 40.3, 60.9, 109.4, 112.0, 112.6, 120.7, 124.1, 129.3, 133.8, 134.7, 175.1; LRMS (ES^-) *m/z*: 320.0 $[M-H]^-$; HRMS (ES^-) calcd. for $C_{15}H_{15}NO_2Br$ $[M-H]^-$ 320.0286, found 320.0288; $[\alpha]_{589}^{25}$ –39.3 (c 0.98, MeOH).

(*R*)-9-(2-Amino-2-oxoethyl)-6-chloro-2,3,4,9-tetrahydro-1H-carbazole-2-carboxylic acid (2a). To a solution of **1k** (163 mg, 0.59 mmol) in dry DMF (1.0 mL) was added Cs_2CO_3 (304 mg, 0.93 mmol) and the suspension stirred at room temperature for 15 min. A solution of iodoacetamide (152 mg, 0.82 mmol) in dry DMF (0.5 mL) was added drop wise and the mixture stirred at 60°C under N_2 overnight. The reaction was quenched with 1 M HCl (20 mL) and extracted with EtOAc (3 x 20 mL). The combined extracts were washed with 0.5 M HCl (2 x 20 mL), brine (20 mL), dried over anhydrous $MgSO_4$ and concentrated. The crude residue was purified by silica gel column chromatography (6:4:0–9:0:1 Et_2O/petrol/MeOH) to give ethyl (*R*)-9-(2-amino-2-oxoethyl)-6-chloro-2,3,4,9-tetrahydro-*1*H-carbazole-2-carboxylate as a yellow powder. The compound was dissolved in absolute EtOH (1 mL) and an aqueous solution of NaOH (2 M, 400 µL) added. The resulting suspension was stirred at room temperature overnight. The reaction mixture was concentrated, diluted with water and washed with CH_2Cl_2 (10 mL). The aqueous layer was acidified with 1 M HCl and extracted with EtOAc (3 x 10 mL). The combined organic extracts were washed with water (10 mL), brine (10 mL), dried over anhydrous $MgSO_4$ and concentrated. The resulting residue was triturated with Et_2O to give **2a** (11 mg, 6% yield) as a white solid: mp > 260°C (dec.); ^{1}H NMR (DMSO-d_6, 500 MHz): δ 1.74–1.76 (1H, m), 2.17–2.20 (1H, m), 2.60–2.63 (1H, m), 2.73–2.92 (4H, m), 4.68 (2H, s), 7.05 (1H, d, *J* = 9.0 Hz), 7.23 (1H, br s), 7.33 (1H, d, *J* = 8.5 Hz), 7.41 (1H, s), 7.53 (1H, br s); ^{13}C NMR (DMSO-d_6, 125 MHz): δ 19.7, 24.0, 25.6, 39.40, 45.2, 107.9, 110.5, 116.7, 120.1, 123.3, 127.7, 135.4, 136.7, 169.4, 176.0; LRMS (ES^+) *m/z*: 329.0 $[M+Na]^+$; HRMS (ES^+) calcd. for $C_{15}H_{16}N_2O_3Cl$ $[M+H]^+$ 307.0849, found 307.0847; $[\alpha]_{589}^{25}$ +10.4 (c 0.6, DMSO).

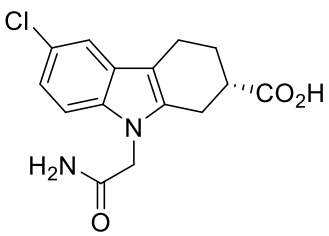

(*S*)-9-(2-Amino-2-oxoethyl)-6-chloro-2,3,4,9-tetrahydro-1H-carbazole-2-carboxylic acid (2b). The compound was prepared according to the method described for **2a** from **1l** (170 mg, 0.61 mmol), iodoacetamide (104 mg, 0.56 mmol) and Cs_2CO_3 (260 mg, 0.80 mmol) in dry DMF (1.5 mL). Following ethyl ester hydrolysis, **2b** (7.4 mg, 4% yield) was obtained as a white powder: mp >

260°C (dec.);^{1}H NMR (DMSO-d_6, 500 MHz): δ 1.74–1.76 (1H, m), 2.18–2.20 (1H, m), 2.61–2.62 (1H, m), 2.77–2.91 (4H, m), 4.68 (2H, s, CH_2), 7.05 (1H, d, J = 8.5 Hz), 7.23 (1H, br s), 7.34 (1H, d, J = 8.0 Hz), 7.40 (1H, s), 7.53 (1H, br s); ^{13}C NMR (DMSO-d_6, 125 MHz): δ 19.7, 24.0, 25.7, 39.5, 45.2, 107.9, 110.6, 116.7, 120.1, 123.3, 127.7, 135.4, 136.7, 169.5, 176.0; LRMS (ES^+) *m/z*: 329.0 $[M+Na]^+$; HRMS (ES^+) calcd. for $C_{15}H_{15}N_2O_3ClNa$ $[M+Na]^+$ 329.0669, found 329.0683; $[\alpha]_{589}^{25}$ –9.2 (c 0.29, DMSO).

(*R*)-2-(6-Bromo-2-(ethoxycarbonyl)-1,2,3,4-tetrahydro-9H-carbazol-9-yl)acetic acid (3a). To a solution of **1m** (642 mg, 2.31 mmol) in dry DMF (1 mL) was added Cs_2CO_3 (581 mg, 1.78 mmol) and *tert*-butyl bromoacetate (302 mg, 1.55 mmol) and the mixture stirred at 60°C under N_2 for 19 h. The reaction mixture was quenched with 1 M HCl (20 mL) and extracted with CH_2Cl_2 (3 x 20 mL). The combined extracts were washed with 0.5 M HCl (3 x 20 mL), brine (20 mL), dried over anhydrous $MgSO_4$ and concentrated. The resulting crude residue was purified by silica gel column chromatography (2:8–5:5 Et_2O/petrol) to give (*R*)-9-(2-(tert-butoxy)-2-oxoethyl)-6-chloro-2,3,4,9-tetrahydro-1H-carbazole-2-carboxylate, which was treated with TFA (1 mL). Following reaction for 1 h, the TFA was evaporated under a stream of N_2 to afford **3a** (402 mg, 83% yield) as a yellow powder: mp 180–182°C; ^{1}H NMR (DMSO-d_6, 500 MHz): δ 1.22 (3H, t, J = 6.8 Hz, CH_3), 1.77–1.78 (1H, m), 2.17–2.19 (1H, m), 2.63–2.94 (5H, m), 4.11–4.15 (2H, m), 4.92 (2H, s), 7.17 (1H, d, J = 8.0), 7.35 (1H, d, J = 8.5 Hz), 7.55 (1H, br s), 13.09 (1H, br s); ^{13}C NMR (DMSO-d_6, 125 MHz): δ 14.1, 19.4, 23.7, 25.6, 39.3, 44.1, 60.2, 108.1, 110.7, 116.8, 120.3, 123.5, 127.7, 135.3, 136.1, 170.3, 174.2; LRMS (ES^-) *m/z*: 380.0 $[M-H]^-$; HRMS (ES^-) calcd. for $C_{17}H_{17}NO_4Br$ 378.0341 $[M-H]^-$, found. 378.0324; $[\alpha]_{589}^{25}$ +25.7 (c 1.00, MeOH).

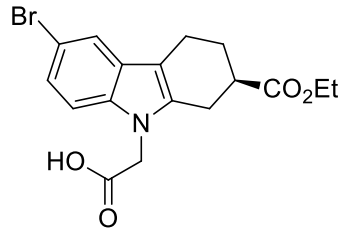

2-(6-Chloro-2-(ethoxycarbonyl)-3,4-dihydro-1H-carbazol-9(2H)-yl)acetic acid (3c). The compound was prepared according to the method described for **3a** from **1k** (642 mg, 2.31 mmol), *tert*-butyl bromoacetate (375 µL, 495 mg, 2.54 mmol) and Cs_2CO_3 (1.03 g, 3.15 mmol) in DMF (4 mL). Following *tert*-butyl ester deprotection **3c** (331 mg, 43% yield) was obtained as an pale yellow powder: mp 180–182°C; ^{1}H NMR (DMSO-d_6, 500 MHz): δ 1.22 (3H, t, J = 7.0 Hz), 1.75–1.80 (1H, m), 2.17–2.19 (1H, m), 2.60–2.65 (1H, m), 2.73–2.94 (4H, m), 4.13 (2H, t, J = 6.8 Hz), 4.92 (2H, d, J = 2.0 Hz), 7.05 (1H, dd, J = 8.5, 1.8 Hz), 7.39 (1H, d, J = 8.5 Hz), 7.41 (1H, d, J = 2.0 Hz), 13.00 (1H, br s); ^{13}C NMR (DMSO-d_6, 125 MHz): δ 14.1, 19.5, 23.7, 25.6, 39.3, 44.1, 60.2, 108.1, 110.7, 116.8, 120.3, 123.5, 127.7, 135.3, 136.1, 170.3, 174.2; LRMS (ES^+) *m/z*: 358.0 $[M+Na]^+$; HRMS (ES^+) calcd. for $C_{17}H_{18}NO_4ClNa$ $[M+Na]^+$ 358.0822, found 358.0815; $[\alpha]_{589}^{25}$ +2.0 (c 0.97, MeOH).

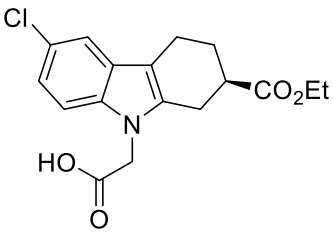

(*R*)-9-(2-Amino-2-oxoethyl)-6-bromo-2,3,4,9-tetrahydro-1H-carbazole-2-carboxylic acid (4a). To a solution of **3a** (87.9 mg, 0.23 mmol) in dry CH_2Cl_2 (2 mL) was added NHS (41 mg, 0.36 mmol) and EDC (79 mg, 0.41mmol) and the reaction mixture stirred for 1 h at room temperature. The CH_2Cl_2 was evaporated under nitrogen and the resulting residue redissolved in THF (2 mL). Aqueous NH_4OH solution (28%; 1 mL) was added and the mixture stirred overnight at room temperature. The resulting precipitate was collected by vacuum filtration (washing with water) and then triturated with Et_2O. The resulting ethyl (*R*)-9-(2-amino-2-oxoethyl)-6-bromo-2,3,4,9-tetrahydro-1H-carbazole-2-carboxylate (29 mg, 0.08 mmol) was dissolved in absolute EtOH (2 mL), an aqueous NaOH solution (2 M; 500 µL) added and the suspension stirred at room temperature overnight. The reaction mixture was concentrated, diluted with water, acidified

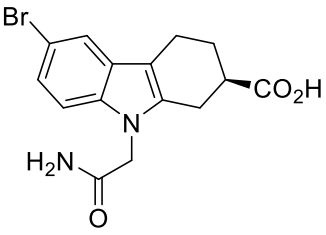

with 1 M HCl and extracted with EtOAc (3 x 10 mL). The combined extracts were washed with water (10 mL), brine (10 mL), dried over anhydrous $MgSO_4$ and concentrated. The resulting crude residue was triturated with Et_2O to give **4a** (12 mg, 14% yield) as a yellow powder: mp > 250°C (dec.); ^{1}H NMR (DMSO-d_6, 300 MHz): δ 1.70–1.76 (1H, m), 2.16–2.20 (1H, m), 2.60–2.92 (5H, m), 4.69 (2H, s), 7.16 (1H, d, *J* = 8.7 Hz), 7.25 (1H, br s), 7.29 (1H, d, *J* = 8.7 Hz), 7.54 (2H, br s), 12.44 (1H, br s); ^{13}C NMR (DMSO-d_6, 75 MHz): δ 19.7, 23.9, 25.6, 39.3, 45.2, 107.8, 111.1, 111.2, 119.7, 122.7, 128.4, 135.6, 136.5, 169.4, 176.0; LRMS (ES^+) *m/z*: 373.0 $[M+Na]^+$; HRMS (ES^+) calcd. for $C_{15}H_{15}N_2O_3BrNa$ $[M+Na]^+$ 373.0164, found 373.0182; $[\alpha]_{589}^{25}$ +12.9 (c 0.64, DMSO).

(*S*)-9-(2-amino-2-oxoethyl)-6-bromo-2,3,4,9-tetrahydro-1H-carbazole-2-carboxylic acid (4b). (*S*)-2-(6-bromo-2-(ethoxycarbonyl)-1,2,3,4-tetrahydro-9H-carbazol-9-yl)acetic acid (**3b**) was prepared according to the method described for **3a** from **1n** (145 g, 0.45 mmol), Cs_2CO_3 (220 mg, 0.67 mmol) and *tert*-butyl bromoacetate (115 mg, 0.59 mmol). Following TFA deprotection of the *tert*-butyl ester, (*S*)-2-(6-bromo-2-(ethoxycarbonyl)-1,2,3,4-tetrahydro-9H-carbazol-9-yl)acetic acid (92 mg, 0.24 mmol) was subsequently reacted with NHS (40 mg, 0.34 mmol) and EDC (72 mg, 0.38 mmol) according to the method described for **4a.** Ethyl ester hydrolysis in an aqueous solution of NaOH (2 M; 300 µL) in absolute ethanol (4 mL) yielded **4b** (28 mg, 33% yield) as a yellow powder: mp > 250°C (dec.); ^{1}H NMR (DMSO-d_6, 500 MHz): δ 1.75–1.76 (1H, m), 2.17–2.20 (1H, m), 2.59–2.62 (1H, m), 2.73–2.92 (4H, m), 4.69 (2H, s, CH_2), 7.16 (1H, d, *J* = 8.5 Hz), 7.23 (1H, br s), 7.29 (1H, d, *J* = 8.5 Hz), 7.52 (1H, br s), 7.54 (1H, s), 12.42 (1H, br s); ^{13}C NMR (DMSO-d_6, 125 MHz): δ 19.7, 23.9, 25.6, 39.3, 45.2, 107.8, 111.1, 111.2, 119.7, 122.7, 128.3, 135.6, 136.5, 169.4, 175.9; LRMS (ES^+) *m/z*: 373.0 $[M+Na]^+$; HRMS (ES^+) calcd. for $C_{15}H_{15}N_2O_3BrNa$ $[M+Na]^+$ 373.0164, found 373.0174; $[\alpha]_{589}^{25}$ +4.4 (c 0.71, DMSO).

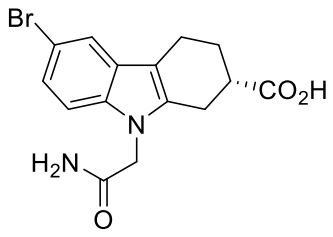

(*R*)-9-(2-((carboxymethyl)amino)-2-oxoethyl)-6-chloro-2,3,4,9-tetrahydro-1H-carbazole-2-carboxylic acid (5a). To a solution containing **3c** (147 mg, 0.44 mmol), glycine methyl ester hydrochloride (69 mg, 0.55 mmol) and HATU (221 mg, 0.58 mmol) in dry DMF (1 mL) was added DIPEA (250 µL, 1.44 mmol) dropwise and the resulting mixture stirred at room temperature overnight under N_2. The reaction mixture was diluted water and extracted with EtOAc (3 x 15 mL). The combined extracts were washed with 0.5 M HCl (3 x 15 mL), sat. $NaHCO_3$ (15 mL) and brine (15 mL) before being dried over anhydrous $MgSO_4$ and concentrated. The resulting residue containing ethyl (*R*)-6-chloro-9-(2-((2-methoxy-2-oxoethyl)amino)-2-oxoethyl)-2,3,4,9-tetrahydro-1H-carbazole-2-carboxylate was dissolved in absolute EtOH (1 mL), an aqueous solution of NaOH (2 M, 400 µL) added and the suspension stirred at room temperature overnight. The reaction mixture was concentrated, diluted with water and then washed with CH_2Cl_2 (15 mL). The aqueous layer was acidified (1 M HCl) and extracted with EtOAc (3 x 15 mL). The combined organic layers were washed with water (15 mL) and brine (15 mL) before being dried over anhydrous $MgSO_4$ and concentrated. The resulting residue was purified by silica gel column chromatography (0:10:0–1:9:0.005 MeOH/CH_2Cl_2/acetic acid) to give **5a** (96 mg, 60% yield) as an off-white powder: mp 220–222°C; ^{1}H NMR (CH_3OD, 500 MHz): δ 1.92–1.99 (1H, m), 2.26–2.29 (1H, m), 2.64–2.70 (1H, m), 2.76–2.79 (1H, m), 2.89–2.98 (3H, m), 3.89 (2H, s), 4.77 (2H, s), 7.04 (1H, d, *J* = 8.5 Hz), 7.23 (1H, d, *J* = 9.0 Hz), 7.35 (1H, s), 7.96 (1H, br s); ^{13}C NMR (CH_3OD, 125 MHz): δ 20.9, 25.2, 27.1, 41.2, 41.8, 46.7, 110.5, 111.0, 118.2, 122.1, 126.1, 129.8, 137.0, 137.2, 171.4, 172.6, 178.6; LRMS (ES^-) *m/z*: 363.0 $[M-H]^-$; HRMS (ES^-) calcd. for $C_{17}H_{16}N_2O_5Cl$ $[M-H]^-$ 363.0748, found 363.0733; $[\alpha]_{589}^{25}$ –5.7 (c 0.50, MeOH).

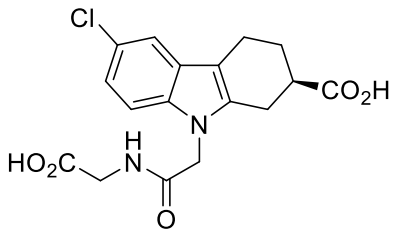

(*R*)-6-bromo-9-(2-((carboxymethyl)amino)-2-oxoethyl)-2,3,4,9-tetrahydro-1H-carbazole-2-carboxylic acid (5b). The compound was prepared according to the method described for **5a** from **3a** (108 mg, 0.28 mmol), glycine methyl ester hydrochloride (49 mg, 0.39 mmol), HATU (137 mg, 0.36 mmol) and DIPEA (160 µL, 0.92 mmol) in dry DMF (1 mL). Following ester deprotection in an aqueous solution of NaOH (2 M; 300 µL) and absolute ethanol (1 mL), **5b** (46 mg, 40% yield) was obtained as an off white powder: mp 238–240°C; ^{1}H NMR (CH_3OD, 500 MHz): δ 1.92–1.95 (1H, m), 2.26–2.28 (1H, m), 2.64–2.68 (1H, m), 2.76–2.79 (1H, m), 2.89–2.98 (3H, m), 3.89 (2H, s), 4.76 (2H, s), 7.17–7.18 (2H, m), 7.50 (1H, s), 8.01 (1H, br s); ^{13}C NMR (CH_3OD, 125 MHz): δ 20.9, 25.1, 27.2, 41.1, 41.8, 46.6, 110.4, 111.5, 113.5, 121.3, 124.7, 130.4, 137.1, 137.3, 171.3, 172.7, 178.6; LRMS (ES^-) *m/z*: 407.0 $[M-H]^-$; HRMS (ES^-) calcd. for $C_{17}H_{16}N_2O_5Br$ $[M-H]^-$ 407.0243, found 407.0256; $[\alpha]_{589}^{25}$ +23.1 (c 0.59, MeOH).

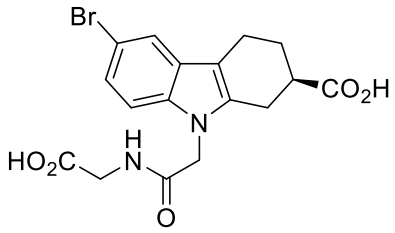

(*R*)-6-chloro-9-(2-(ethylamino)-2-oxoethyl)-2,3,4,9-tetrahydro-1H-carbazole-2-carboxylic acid (5c). The compound was prepared according to the method described for **5a** from **3c** (140 mg, 0.42 mmol), ethylamine hydrochloride (46 mg, 0.56 mmol), HATU (211 mg, 0.56 mmol) and DIPEA (200 µL, 1.15 mmol) in dry DMF (1 mL). Ester deprotection in an aqueous solution of NaOH (2 M; 400 µL) and absolute ethanol (1 mL) afforded **5c** (54 mg, 38% yield) as an off-white powder: mp 246–248°C; ^{1}H NMR (DMSO-d_6, 500 MHz): δ 1.02 (3H, t, *J* = 7.0 Hz), 1.75–1.76 (1H, m), 2.17–2.20 (1H, m), 2.61–2.62 (1H, m), 2.77–2.93 (4H, m), 3.08–3.12 (2H, m), 4.69 (2H, s), 7.05 (1H, d, *J* = 8.0 Hz), 7.34 (1H, d, *J* = 9.0 Hz), 7.40 (1H, s), 8.12 (1H, s), 12.43 (1H, br s); ^{13}C NMR (DMSO-d_6, 125 MHz): δ 14.6, 19.7, 24.1, 25.6, 33.5, 39.6, 45.6, 108.0, 110.6, 116.7, 120.1, 123.3, 127.7, 135.4, 136.7, 167.0, 176.0; LRMS (ES^+) *m/z*: 357.0 $[M+Na]^+$; HRMS (ES^+) calcd. for $C_{17}H_{19}N_2O_3ClNa$ $[M+Na]^+$ 357.0982, found 357.0970; $[\alpha]_{589}^{25}$ +2.7 (c 0.52, MeOH).

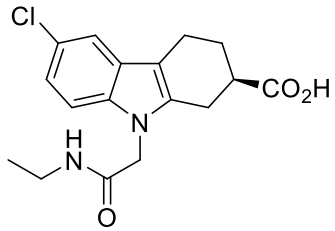

(*R*)-9-(2-((4-(2-amino-2-oxoethyl)phenyl)amino)-2-oxoethyl)-6-chloro-2,3,4,9-tetrahydro-1H-carbazole-2-carboxylic acid (5d). The compound was prepared according to the method described for **5a** from **3c** (125 mg, 0.37 mmol), 2-(4-aminophenyl)acetamide (73 mg, 0.48 mmol), HATU (181 mg, 0.48 mmol) and DIPEA (230 µL, 1.32 mmol) in dry DMF (1 mL). Ester deprotection in an aqueous solution of NaOH (2 M; 140 µL) and absolute ethanol (1 mL) gave **5d** (29 mg, 31% yield) as a white powder: mp > 260°C (dec.);^{1}H NMR (DMSO-d_6, 500 MHz): δ 1.76–1.78 (1H, m), 2.18–2.20 (1H, m), 2.63–2.96 (5H, m), 3.31 (2H, s), 4.95 (2H, s), 6.82 (2H, s), 7.06 (1H, d, *J* = 7.5 Hz), 7.19 (2H, d, *J* = 8.0 Hz), 7.39–7.42 (2H, m), 7.49 (2H, d, *J* = 8.0 Hz), 10.34 (1H, s), 12.50 (1H, br s); ^{13}C NMR (DMSO-d_6, 125 MHz): δ 19.7, 24.0, 25.7, 39.3, 41.7, 46.0, 108.1, 110.6, 116.8, 119.1, 120.2, 123.4, 127.7, 129.4, 131.7, 135.5, 136.8, 136.9, 166.1, 172.2, 176.0; LRMS (ES^-) *m/z*: 438.0 $[M-H]^-$; HRMS (ES^-) calcd. for $C_{23}H_{21}N_3O_4Cl$ $[M-H]^-$ 438.1221, found 438.1215; $[\alpha]_{589}^{25}$ +3.77 (c 0.53, DMSO).

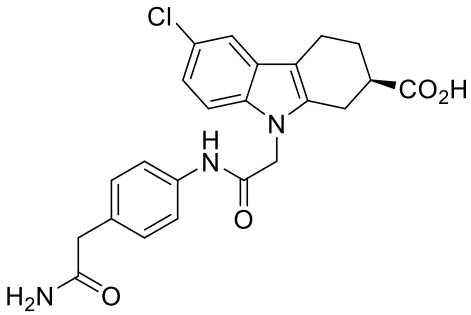

(*R*)-6-bromo-9-(2-(((1-(BOC)piperidin-4-yl)methyl)amino)-2-oxoethyl)-2,3,4,9-tetrahydro-1H-carbazole-2-carboxylic acid (5e). The compound was prepared according to the method described for **5a** from **3a** (216 mg, 0.57 mmol), *tert*-butyl 4-(aminomethyl)piperidine-1-carboxylate (159 mg, 0.74 mmol), HATU (301 mg, 0.79 mmol) and DIPEA (350 µL, 2.01 mmol) in dry DMF (2 mL). Ester deprotection in an aqueous solution of NaOH (2 M; 300 µL) and absolute ethanol (1 mL) provided **5e** (68 mg, 36% yield) as a

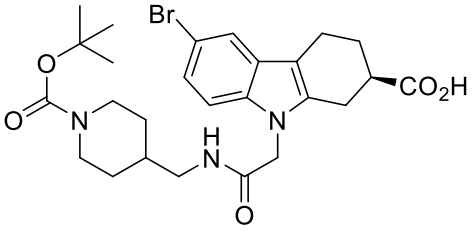

pale yellow powder: mp 158–160°C; ^{1}H NMR (DMSO-d_6, 500 MHz): δ 0.95–0.99 (2H, m), 1.39 (9H, s), 1.57–1.59 (3H, m), 1.74–1.77 (1H, m), 2.17–2.20 (1H, m), 2.61–2.64 (3H, m), 2.73–2.91 (3H, m), 2.94–2.97 (3H, m), 3.91 (2H, br d, *J* = 9.5 Hz), 4.72 (2H, s), 7.16 (1H, dd, *J* = 9.0, 1.8 Hz), 7.30 (1H, d, *J* = 9.0 Hz), 7.54 (1H, d, *J* = 1.5 Hz), 8.16 (1H, br t, *J* = 5.8 Hz), 12.44 (1H, br s); ^{13}C NMR (DMSO-d_6, 125 MHz): δ 19.7, 24.0, 25.7, 28.1, 29.4, 35.7, 39.4, 44.0, 45.5, 78.5, 107.9, 111.2, 111.3, 119.8, 122.8, 128.4, 135.6, 136.6, 153.8, 167.5, 176.0; LRMS (ES$^+$) *m/z*: 570.0 [M+Na]$^+$; HRMS (ES$^+$) calcd. for $C_{26}H_{34}N_3O_5BrNa$ [M+Na]$^+$ 570.1580, found 570.1604; $[\alpha]_{589}^{25}$ +8.5 (c 0.52, MeOH).

(*R*)-6-bromo-9-(2-oxo-2-((piperidin-4-ylmethyl)amino)ethyl)-2,3,4,9-tetrahydro-1H-carbazole-2-carboxylic acid.TFA salt (5f). Neat TFA (1 mL) was added to **5e** (42 mg, 0.076 mmol) and the mixture stirred at room temperature for 1 h. The TFA was evaporated under a stream of N_2 and the resulting residue triturated with petrol to give **5f** (39 mg, 91% yield) as a yellow powder: mp 212–214°C; ^{1}H NMR (CH_3OD, 500 MHz): δ 1.29–1.37 (2H, m), 1.77–1.84 (3H, m), 1.98–1.99 (1H, m), 2.27–2.30 (1H, m), 2.70–2.81 (2H, m), 2.89–2.94 (5H, m), 3.13 (2H, d, *J* = 6.0 Hz), 3.31–3.36 (2H, m), 4.76 (2H, d, *J* = 3.0 Hz), 7.19 (2H, br s), 7.54 (1H, s); ^{13}C NMR (CH_3OD, 125 MHz): δ 20.8, 25.3, 27.1, 27.6, 35.2, 41.0, 44.8, 45.0, 46.8, 110.4, 111.4, 113.5, 121.4, 124.7, 130.5, 137.1, 137.3, 171.0, 178.5; LRMS (ES$^+$) *m/z*: 448.0 [M+H]$^+$; HRMS (ES$^+$) calcd. for $C_{21}H_{27}N_3O_3Br$ [M+H]$^+$ 448.1236, found 448.1222; $[\alpha]_{589}^{25}$ +4.6 (c 0.51, MeOH).

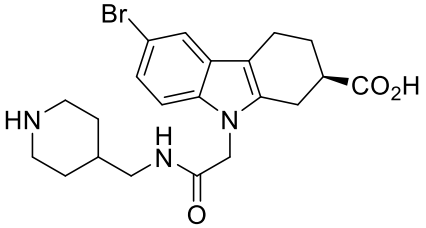

(*R*)-9-(2-((2-amino-2-oxoethyl)amino)-2-oxoethyl)-6-bromo-2,3,4,9-tetrahydro-1H-carbazole-2-carboxylic acid (5g). The compound was prepared according to the method described for **5a** from **3a** (122 mg, 0.32 mmol), glycinamide hydrochloride (60 mg, 0.55 mmol), HATU (166 mg, 0.44 mmol) and DIPEA (230 µL, 1.32 mmol) in dry DMF (1 mL). Ester hydrolysis in an aqueous solution of NaOH (2 M; 300 µL) and absolute ethanol (1 mL) afforded **5g** (8.5 mg, 6.5% yield) as an off-white powder: mp 232–234°C; ^{1}H NMR (DMSO-d_6, 500 MHz): δ 1.74–1.76 (1H, m), 2.17–2.19 (1H, m), 2.61–2.63 (1H, m), 2.73–2.95 (4H, m), 3.66 (2H, d, *J* = 5.5 Hz, CH_2), 4.80 (2H, s, CH_2), 7.05 (1H, s), 7.15 (1H, d, *J* = 8.5 Hz), 7.31–7.35 (2H, m), 7.54 (1H, s), 8.26 (1H, br s), 12.40 (1H, br s); ^{13}C NMR (DMSO-d_6, 125 MHz): δ 19.6, 23.9, 25.7, 39.8, 41.8, 45.3, 107.9, 111.2, 119.7, 122.7, 128.4, 135.6, 136.6, 167.7, 170.4, 175.9; LRMS (ES$^-$) *m/z*: 408.0 [M-H]$^-$; HRMS (ES$^-$) calcd. for $C_{17}H_{17}N_3O_4Br$ [M-H]$^-$ 406.0402, found 406.0404; $[\alpha]_{589}^{25}$ –9.6 (c 0.19, DMSO).

(*R*)-6-bromo-9-(2-((4-carbamoylbenzyl)amino)-2-oxoethyl)-2,3,4,9-tetrahydro-1H-carbazole-2-carboxylic acid (5h). The compound was prepared according to the method described for **5a** from **3a** (155 mg, 0.41 mmol), 4-(aminomethyl)benzamide (74 mg, 0.49 mmol), HATU (227 mg, 0.60 mmol) and DIPEA (250 µL, 1.44 mmol) in dry DMF (1 mL). Following ester deprotection in an aqueous solution of NaOH (2 M; 300 µL) and absolute ethanol (1 mL), the mixture was acidified and the resulting precipitate collected by vacuum filtration. The precipitate was basified with 1 M NaOH, dissolved in water and filtered through a 1 cm plug

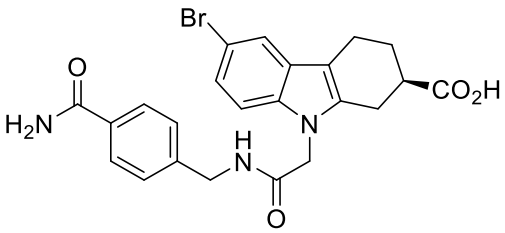

of reverse phase silica, washing with water. The aqueous solution was acidified and the precipitate collected by vacuum filtration, washing with ethanol and petrol to give **5h** (7.0 mg, 4% yield) as an off-white powder: mp > 230°C (dec); ^{1}H NMR (DMSO-d_6, 500 MHz): δ 1.75–1.77 (1H, m), 2.18–2.20 (1H, m), 2.62–2.63 (1H, m), 2.73–2.97 (4H, m), 4.34 (2H, s), 4.83 (2H, s), 7.17 (1H, br s), 7.28–7.38 (4H, m), 7.55 (1H, s), 7.82 (2H, d, *J* = 7.5 Hz), 7.93 (1H, br s), 8.78 (1H, br s), 12.44 (1H, br s); ^{13}C NMR (DMSO-d_6, 125 MHz): δ 19.7, 24.1, 25.7, 40.2, 42.0, 45.6, 108.1, 111.2, 111.4, 119.8, 122.8, 126.9, 127.6, 128.5, 132.9, 135.7, 136.6, 142.5, 167.7, 176.1; LRMS (ES$^-$) *m/z*: 482.0 [M-H]$^-$; HRMS (ES$^-$) calcd. for $C_{23}H_{21}N_3O_4Br$ [M-H]$^-$ 482.0715, found 482.0717; $[\alpha]_{589}^{25}$ +7.4 (c 0.48, DMSO).

(*R*)-9-(2-((1-(2-amino-2-oxoethyl)piperidin-4-yl)amino)-2-oxoethyl)-6-bromo-2,3,4,9-tetrahydro-1H-carbazole-2-carboxylic acid potassium salt (5i). The compound was prepared according to the method described for **5a** from **3a** (83 mg, 0.22 mmol), 2-(4-amino-1-piperidinyl) acetatmide dihydrochloride (70 mg, 0.25 mmol), HATU (111 mg, 0.29 mmol) and DIPEA (200 µL, 1.15 mmol) in dry DMF (1 mL). Following deprotection in an aqueous solution of KOH (1 M, 38 µL, 0.038 mmol) in THF:EtOH:H_2O (1:1:1; 1 mL) the mixture was concentrated, washed with CH_2Cl_2 (2 x 2 mL) and the aqueous layer lyophilized. The resulting residue was triturated with ether, redissolved in methanol, filtered and concentrated to give the potassium salt of **5i** (13 mg, 64% yield) as an off-white gum: ^{1}H NMR (DMSO-d_6, 500 MHz): δ 1.47–1.52 (2H, m), 1.68–1.71 (3H, m), 2.06–2.11 (3H, m), 2.27–2.29 (1H, m), 2.48–2.50 (1H, m), 2.65–2.73 (5H, m), 2.81 (2H, s), 3.49–3.51 (1H, m), 4.67 (2H, d, *J* = 3.5 Hz), 7.09–7.11 (2H, m), 7.16 (1H, br s), 7.25 (1H, d, *J* = 8.5 Hz), 7.46 (1H, d, *J* = 2.0 Hz), 8.28 (1H, br d, *J* = 7.0 Hz); ^{13}C NMR (DMSO-d_6, 125 MHz): δ 20.4, 25.6, 27.2, 31.2, 43.0, 45.5, 45.8, 52.1, 61.4, 108.1, 110.9, 119.4, 122.0, 128.8, 135.0, 139.2, 166.7, 171.9, 177.4; LRMS (ES$^+$) *m/z*: 491.0 [M-K+H]$^+$; HRMS (ES$^+$) calcd. for $C_{22}H_{28}N_4O_4Br$ [M-K+H]$^+$ 491.1294, found 491.1310; $[\alpha]_{589}^{25}$ –4.3 (c 1.28, MeOH).

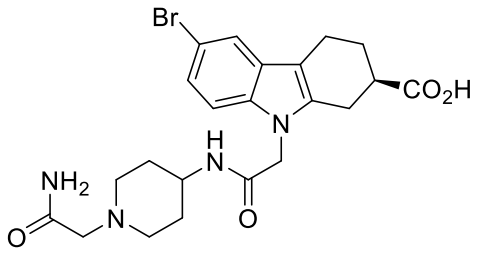

(*R*)-6-bromo-9-(2-(((R)-5-((tert-butoxycarbonyl)amino)-1-carboxypentyl)amino)-2-oxoethyl)-2,3,4,9-tetrahydro-1H-carbazole-2-carboxylic acid (5j). The compound was prepared according to the method described for **5a** with the following modification. Compound **3a** (96 mg, 0.25 mmol) was pre-activated with HATU (136 mg, 0.36 mmol) and DIPEA (160 µL, 0.92 mmol) in dry CH_2Cl_2 (1 mL) containing a few drops of DMF, before a solution of NH_2-(D)-Lys-(BOC)-O^{t}Bu.HCl (107 mg, 0.32 mmol) in dry CH_2Cl_2 (1 mL) was added. Ester deprotection with LiOH.H_2O (27 mg, 0.63 mmol) in THF:EtOH:H_2O (1:1:1; 1 mL) yielded **5j** (98 mg, 57% yield) as a yellow solid: mp 78–80°C; ^{1}H NMR (DMSO-d_6, 500 MHz): δ 1.28 (4H, br s), 1.38 (9H, s), 1.59–1.61 (1H, m), 1.71–1.72 (2H, m), 2.17–2.18 (1H, m), 2.61–2.96 (7H, m), 4.14 (1H, br s), 4.74–4.80 (2H, m), 6.75 (1H, br s), 7.16 (1H, d, *J* = 8.5 Hz), 7.31 (1H, t), 7.54 (1H, s), 8.48 (1H, t), 12.54 (1H, br s); ^{13}C NMR (DMSO-d_6, 75 MHz): δ 19.7, 22.7, 24.0, 25.7, 28.3, 29.1, 30.8, 39.4, 39.8, 45.2, 52.1, 77.4, 107.9, 111.2, 111.3, 119.7, 122.7, 128.4, 135.6, 136.6, 155.6, 167.5, 173.4, 176.0; LRMS (ES$^-$) *m/z*: 580.0 [M-H]$^-$; HRMS (ES$^-$) calcd. for $C_{26}H_{33}N_3O_7Br$ [M-H]$^-$ 578.1502, found 578.1504; $[\alpha]_{589}^{25}$ +2.4 (c 2.84, MeOH).

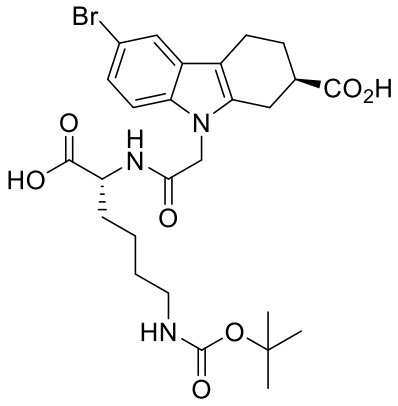

(*R*)-6-bromo-9-(2-(((S)-1-carboxy-3-methylbutyl)amino)-2-oxoethyl)-2,3,4,9-tetrahydro-1H-carbazole-2-carboxylic acid (5k). The compound was prepared according to the method described for **5a** from **3a**

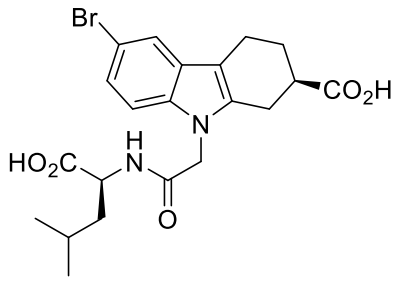

(249 mg, 0.654 mmol), NH_2-(L)-Leu-(O^{t}Bu).HCl (194 mg, 0.87 mmol), HATU (339 mg, 0.891 mmol) and DIPEA (450 µL, 2.58 mmol) in dry DMF (5 mL). Following ethyl ester hydrolysis in an aqueous solution of NaOH (2 M; 500 µL) in EtOH:H_2O (1:1; 3 mL), the resulting residue was treated with TFA (1 mL) and the mixture stirred for 1 h. Removal of the TFA under a stream of N_2 and trituration of the residue with toluene gave **5k** (39 mg, 30% yield); ^{1}H NMR (CD_3OD, 500 MHz): δ 0.82–0.90 (6H, m), 1.25 (1H, br s), 1.52–1.59 (2H, m), 1.86–1.93 (1H, m), 2.25–2.28 (1H, m), 2.63–2.69 (1H, m), 2.74–2.78 (1H, m) 2.86–2.93 (3H, m), 4.23–4.37 (1H, m), 4.76 (2H, s), 7.13 (1H, d, *J* = 9.0 Hz), 7.16 (1H, d, *J* = 8.5 Hz), 7.48 (1H, s); ^{13}C NMR (CD_3OD, 125 MHz): δ 21.0, 23.5, 25.4, 26.1, 27.1, 41.5, 46.6, 49.2, 52.1, 110.3, 111.7, 113.5, 121.5, 124.5, 130.5, 137.2, 137.4, 170.8, 175.6, 178.6; LRMS (ES^-) *m/z*: 465.0 $[M-H]^-$; HRMS (ES^-) calcd. for $C_{22}H_{20}N_6OBr$ $[M–H]^-$ 463.0882, found 463.0879; $[\alpha]_{589}^{25}$+5.22 (c 0.46, MeOH).

(*R*)-6-bromo-9-(2-(((*R*)-1-carboxy-2-phenylethyl)amino)-2-oxoethyl)-2,3,4,9-tetrahydro-1H-carbazole-2-carboxylic acid (5l).

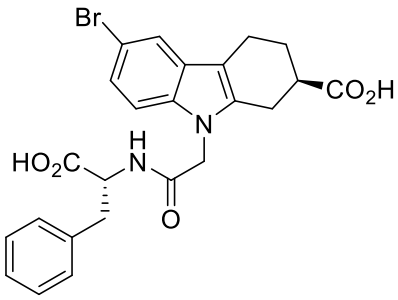

The compound was prepared according to the method described for **5a** from **3a** (134 mg, 0.35 mmol), NH_2-(D)-Phe-(OMe).HCl (92 mg, 0.43 mmol), HATU (173 mg, 0.46 mmol) and DIPEA (230 µL, 1.32 mmol) in dry DMF (1 mL). Global ester deprotection in an aqueous solution of NaOH (2 M; 300 µL) and absolute ethanol (2 mL) afforded **5l** (69 mg, 39% yield) as an off-white powder: mp 194-196 °C; ^{1}H NMR (DMSO-*d*$_6$, 500 MHz): δ 1.72-1.73 (1H, m), 2.15 (1H, m), 2.58-2.86 (5H, m), 2.86-2.90 (1H, m), 3.06-3.09 (1H, m), 4.41 (1H, br s), 4.65-4.77 (2H, m), 7.11-7.25 (7H, m), 7.52 (1H, s), 8.36 (1H, br s), 12.70 (1H, br s); ^{13}C NMR (DMSO-*d*$_6$, 125 MHz): δ 19.6, 23.8, 25.6, 36.7, 45.1, 53.4, 53.5, 107.9, 111.2, 111.3, 1119.7, 122.7.7, 126.5, 128.2, 128.4, 129.1, 135.5, 136.4, 137.3, 167.3, 172.6, 175.9; LRMS (ES^+) *m/z*: 522.9 $[M+Na]^+$; HRMS (ES^+) calcd. for $C_{24}H_{23}N_2O_5BrNa$ $[M+Na]^+$ 521.0688, found 521.0686; $[\alpha]_{589}^{25}$ -22.9 (c 0.52, MeOH).

(*R*)-6-bromo-9-(2-(((*S*)-1-carboxy-2-phenylethyl)amino)-2-oxoethyl)-2,3,4,9-tetrahydro-1H-carbazole-2-carboxylic acid (5m). The compound was prepared according to the method described for **5a** from **3a**

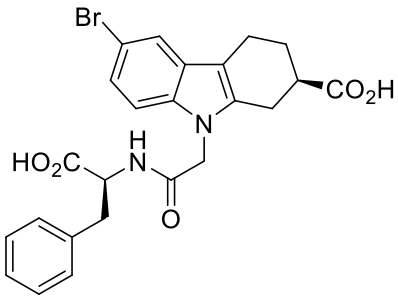

(129 mg, 0.34 mmol), NH_2-(L)-Phe-(OMe).HCl (84 mg, 0.39 mmol), HATU (163 mg, 0.43 mmol) and DIPEA (200 µL, 1.15 mmol) in dry DMF (1 mL). Global ester deprotection in an aqueous solution of NaOH (2 M; 300 µL) and H_2O:EtOH (1:1; 2 mL) gave **5m** (98 mg, 57% yield) as a yellow solid: mp 208–210°C; ^{1}H NMR (DMSO-*d*$_6$, 500 MHz): δ 1.73–1.75 (1H, m), 2.16 (1H, m), 2.59–2.60 (1H, m), 2.70–2.76 (3H, m), 2.87–2.93 (2H, m), 3.08–3.11 (1H, m), 4.47–4.84 (1H, m, CH), 4.66–4.78 (2H, m), 7.12–7.29 (7H, m), 7.53 (1H, s), 8.44–8.46 (1H, m), 12.63 (1H, br s); ^{13}C NMR (DMSO-*d*$_6$, 125 MHz): δ 19.6, 23.8, 25.7, 36.7, 39.4, 45.1, 53.3, 107.9, 111.2, 111.3, 119.7, 122.7, 126.5, 128.2, 128.4, 129.1, 135.5, 136.5, 137.3, 167.3, 172.6, 175.9; LRMS (ES^+) *m/z*: 521.0 $[M+Na]^+$; HRMS (ES^+) calcd. for $C_{24}H_{23}N_2O_5BrNa$ $[M+Na]^+$ 521.0688, found 521.0710; $[\alpha]_{589}^{25}$ +17.8 (c 0.48, MeOH).

Supplementary References

(1) Georgescu, R. E.; Yurieva, O.; Kim, S. S.; Kuriyan, J.; Kong, X.-P.; O'Donnell, M. *Proc. Natl. Acad. Sci. U. S. A.* **2008**, *105*, 11116.

(2) Wijffels, G.; Johnson, W. M.; Oakley, A. J.; Turner, K.; Epa, V. C.; Briscoe, S. J.; Polley, M.; Liepa, A. J.; Hofmann, A.; Buchardt, J.; Christensen, C.; Prosselkov, P.; Dalrymple, B. P.; Alewood, P. F.; Jennings, P. A.; Dixon, N. E.; Winkler, D. A. *J. Med. Chem.* **2011**, *54*, 4831.

(3) Otwinowski, Z.; Minor, W. *Methods Enzymol.* **1997,** *276*, 307.

(4) Mortenson, P. N.; Murray, C. W. *J. Comput. Aided Mol. Des.* **2011**, *25*, 663.

(5) Papadopoulos, J. S.; Agarwala, R. *Bioinformatics* **2007**, *23*, 1073.

(6) Berger, L.; Corraz, A. J.; Hoffmann-La Roche Inc.: 1977; Vol. US4009181 A.

(7) Napper, A. D.; Hixon, J.; McDonagh, T.; Keavey, K.; Pons, J.-F.; Barker, J.; Yau, W. T.; Amouzegh, P.; Flegg, A.; Hamelin, E.; Thomas, R. J.; Kates, M.; Jones, S.; Navia, M. A.; Saunders, J. O.; DiStefano, P. S.; Curtis, R. *J. Med. Chem.* **2005**, *48*, 8045.